MOLECULAR BIOLOGY

HnRNP C binding to inverted *Alu* elements protects the transcriptome from pre-mRNA circularization

Alberto Marini[1,2]†‡, Consuelo Pitolli[1,2]†, Sabrina Ciccone[1], Marco Pieraccioli[1,2], Noémie Robil[3], Chiara Naro[1,2], Fernando Palluzzi[4]§, Manuela Giansanti[5], Gianpiero Tamburrini[1,6], Luciano Giacò[4], Pierre de la Grange[3], Francesca Nazio[7], Pamela Bielli[8], Claudio Sette[1,2], Vittoria Pagliarini[1,2]*

Back-splicing is a noncanonical splicing event driving circular RNA (circRNA) biogenesis. While its molecular mechanisms are partly known, global regulation in tumors remains unclear. Here, we uncover an hnRNP C–dependent mechanism that represses a broad repertoire of circRNAs in group 3 medulloblastoma (MB). HnRNP C binds *Alu* elements, preventing pre-mRNA circularization. Expression of hnRNP C modulates the balance between linear and circular splicing, ensuring efficient expression of genes that sustain the oncogenic phenotype of group 3 MB cells. In the absence of hnRNP C, introns flanking the circularizing exons generate cytoplasmic double-stranded RNAs via inverted *Alu* base pairing, triggering an interferon-induced antiviral response. These findings unveil hnRNP C as a guardian of transcriptome integrity by repressing circRNA biogenesis. Last, targeting hnRNP C in group 3 MB may trigger an inflammatory immune response, thereby boosting cancer surveillance.

INTRODUCTION

Circular RNAs are covalently closed molecules generated by a back-splicing reaction in the precursor mRNAs (pre-mRNAs) (*1*). Back-splicing involves the splicing between a downstream 5′ splice site with an upstream 3′ splice site and, as canonical linear splicing, is mediated by the spliceosome machinery and regulated by similar sequence elements and RNA binding proteins (RBPs) (*1*–*3*). The resulting circRNAs are generally more stable than their linear counterparts and have been shown to affect many biological processes, ranging from transcription to translation of target mRNAs or protein functions in both nucleus and the cytoplasm (*1*–*3*). Notably, the dysregulation of circRNA expression has been linked to many human diseases, particularly to human cancers (*3*, *4*).

Introns that flank circularizing exons are generally characterized by increased length and are enriched in inverted *Alu* repeat elements (*1*–*3*). These elements are essential to form a transient *Alu* pairing-mediated double-stranded RNA (dsRNA) between the involved introns, thus bringing into proximity back-splicing sites that are otherwise distant from each other and favoring the back-splicing event (*1*–*3*, *5*). In addition to inverted *Alu* sequences, RBPs also play a fundamental regulatory role in circRNA biogenesis by binding in proximity of back-splicing sites and modulating the efficiency of the reaction (*6*–*9*). Thus, it is conceivable that the specific repertoire of RBPs greatly influences the circRNAs that are expressed into each given cell. The alteration of this balance often occurs in disease states, such as cancer, where the expression of RBPs is often deregulated (*10*). In this context, RBPs have been shown to either promote the expression of oncogenic circRNAs or, alternatively, to inhibit circRNA biogenesis, thus ensuring the proper processing and expression of protumoral linear transcripts that are essential for tumor cell survival. Mounting evidence suggests that tumors are characterized by a global down-regulation of circRNA expression with respect to healthy tissues (*11*, *12*). Here, we found that the RBP hnRNP C is a critical regulator of the balance of circRNA biogenesis in the context of medulloblastoma (MB), the most common malignant brain tumor of childhood (*13*, *14*). Notably, MB arises in the cerebellum, the brain region with the highest expression levels of circRNAs (*15*). Among the different MB subgroups, group 3 displays the most aggressive phenotype and shorter survival (*13*, *14*). Amplification and/or overexpression of the oncogenic transcription factor MYC drives an abnormal transcriptional program in group 3 MB cells. MYC-amplified tumors are characterized by an increased transcriptional rate and accumulation of nascent pre-mRNAs in the nucleus, thus imposing a stress to the splicing machinery (*16*). As a consequence, MYC-amplified tumor cells are generally dependent on an efficient splicing machinery for their survival (*16*). To support the splicing machinery, MYC promotes the expression of a vast repertoire of splicing factors in many tumor cell types (*17*–*20*). Because linear splicing and back-splicing compete for the same pre-mRNA (*21*–*23*), it is conceivable that the global repression of circRNA biogenesis in tumor cells fuels the increased output of canonical mRNAs in high demanding tumor cells, such as those harboring amplification of MYC. Thus, we reasoned that the regulatory mechanism(s) controlling the extent of circRNA biogenesis might be particularly exacerbated in MYC-amplified group 3 MB. In line with this hypothesis, RNA sequencing (RNA-seq) analysis of samples from patients with high-risk group 3 MB revealed a strong down-regulation of circRNAs with respect to healthy individuals. Motif enrichment analyses and functional studies demonstrated that hnRNP C exerts a widespread inhibitory effect on circRNA biogenesis in group 3 MB cells while concomitantly supporting the expression of cognate linear transcripts. Mechanistically, we show that hnRNP C preferentially binds proximal intronic *Alu* elements that flank the circularizing exons, thus inhibiting the occurrence

[1]Department of Neuroscience, Section of Human Anatomy, Università Cattolica del Sacro Cuore, 00168 Rome, Italy. [2]GSTEP-Organoids Research Core Facility, IRCCS Fondazione Policlinico Universitario Agostino Gemelli, 00168 Rome, Italy. [3]Genosplice, Paris, France. [4]Bioinformatics Research Core Facility, Gemelli Science and Technology Park (GSTeP), IRCCS Fondazione Policlinico Universitario Agostino Gemelli, 00168 Rome, Italy. [5]Innate Lymphoid Cells Unit, Bambino Gesù Children's Hospital IRCCS, Rome, Italy. [6]Pediatric Neurosurgery, IRCCS Fondazione Policlinico Universitario Agostino Gemelli, 00168 Rome, Italy. [7]Department of Biology, University of Rome Tor Vergata, 00133 Rome, Italy. [8]Department of Biomedicine and Prevention, University of Rome Tor Vergata, 00133 Rome, Italy.
*Corresponding author. Email: vittoria.pagliarini@unicatt.it
†These authors contributed equally to this work.
‡Present address: Laboratory of Cutaneous Physiopathology, Integrated Center of Metabolomics Research, San Gallicano Dermatological Institute, IRCCS, 00144 Rome, Italy.
§Present Address: Integrated Omics Department, Novo Nordisk, 2860 Søborg, Denmark.

of the back-splicing event. In the absence of hnRNP C, paired intronic dsRNAs are stabilized and, after the back-splicing reaction, eventually accumulate into the cytoplasm and trigger the activation of the innate immune response, contributing to the reduced fitness of MB cells. Together, our findings uncover a functional role of hnRNP C as a general negative regulator of circRNA biogenesis and suggest the existence of an hnRNP C–dependent safeguard mechanism to repress aberrant circularization of pre-mRNAs in MYC-amplified tumors.

RESULTS

CircRNA expression is extensively down-regulated in patients with group 3 MB

Large transcriptomic analyses in different types of cancers, including MB, highlighted a significant down-regulation of circRNAs compared to normal tissues (*11*, *12*). This observation suggests a functional correlation between repression of circRNA biogenesis and tumorigenesis. To identify and quantify circRNAs expressed in high-risk group 3 MB, we searched for back-splicing junctions (BSJs) by querying RNA-seq data downloaded from the International Cancer Genome Consortium Controlled Data Portal (dataset EGAD00001004958). We compared 16 group 3 MBs with 4 fetal cerebella (FC) and 5 adult cerebella (AC), thus including both undifferentiated and differentiated healthy tissues (table S1). Computational analyses carried out with CircExplorer2 and CircRNA Identifier (CIRI), two widely used tools for circRNA detection (*24*, *25*), identified 12,343 BSJs expressed in at least one of the experimental groups, with 3444 high confidence events supported by both tools (Fig. 1A and table S2). Among these common BSJs, more than 90% are predicted to yield exonic circRNAs (fig. S1A). While a fraction of these BSJs ($n = 923$; 26.8%) were detected in at least two experimental groups, the majority ($n = 2521$; 73.1%) were specifically detected only in one of them (Fig. 1B and table S2). Most of these unique BSJs were detected either in the AC ($n = 1461$) or in the MB ($n = 880$) samples. The differential expression analysis of BSJs in these two groups showed that circRNAs are mostly down-regulated in our cohort of group 3 MB patients compared to AC (Fig. 1C and table S3), while no differences were observed with respect to FC (fig. S1B and table S4).

To investigate whether the suppression of circRNA biogenesis in group 3 MB is an active regulatory mechanism, we explored the trans-acting factors that are potentially involved in back-splicing modulation. To this end, we searched for RNA sequence motifs enriched in the introns flanking the back-spliced exons of AC-unique circRNAs ($n = 1461$; Fig. 1B). Using the MEME suite tool (*26*), we compared the sequence of regions encompassing 100-nt upstream of the 3′ splice sites or downstream of the 5′ splice sites, involved in the circularization of AC-unique exons, with the corresponding intronic regions not involved in back-splicing events (~180,000 intron sequences; UCSC genome browser, https://genome.ucsc.edu; Fig. 1D and table S5). Simple, Thorough, Rapid, Enriched Motif Elicitation (STREME) analysis (*27*) identified putative consensus motifs enriched near the unique AC BSJs, while the TomTom Motif Comparison tool (*28*, *29*) predicted the RBPs that potentially bind these motifs (Fig. 1E). Taking into consideration the top 3 most significantly enriched motifs upstream and downstream the BSJs, we identified nine nuclear RBPs (KHDRBS1/Sam68, SART3, RBM41, A1CF, ZCRB1, KHDRBS2/SLM1, KHDRBS3, HNRNPC, and HNRNPCL1) as potential regulators of AC unique exons back-splicing (Fig. 1E). Next, to identify MB-specific RBPs involved in the biogenesis of these circRNAs, we focused on RBPs that were significantly up-regulated in our cohort of group 3 MB patients compared to healthy individuals (Fig. 1F, fig. S1C, and table S6). Based on these inclusion criteria, we selected HNRNPC, KHDRBS1/Sam68, SART3, and KHDRBS2/SLM1 for subsequent analysis. Notably, all these RBPs showed the highest protein expression in MB compared to other pediatric brain tumors analyzed (fig. S1, D to G), further suggesting their involvement in this cancer type. Gene expression analysis in public MB datasets confirmed the up-regulation of hnRNP C, SART3, Sam68, and SLM1 in group 3 MB ($n = 233$) compared to normal cerebellum ($n = 291$). By contrast, SLM1 was preferentially up-regulated in groups 3 and 4 MB respect to Sonic Hedgehog (SHH) and WNT MB (fig. S1, H to K). hnRNP C and SART3 are the only RBP specifically up-regulated in patients with group 3 MB also with respect to the other MB subgroups [group 4, SHH and Wingless (WNT)] (fig. S1, G and H).

HnRNP C represses the expression of circRNAs in group 3 MB cells

Previous studies reported a role for hnRNP C and Sam68 in the regulation of circRNA biogenesis (*7*, *30*), whereas no information is available for SART3 and SLM1. To validate the functional role of the selected RBPs in circRNA biogenesis in group 3 MB cells, we knocked down their expression in D341-Med (hereafter D341) and HD-MB03 cells. Silencing efficiency was evaluated by Western blotting for hnRNP C, SART3 and Sam68 (Fig. 2A and fig. S2B) whereas, due to cross-reactions of the SLM1 antibody with the highly homologous Sam68 (Fig. 2A and fig. S2B), SLM1 expression was evaluated by quantitative polymerase chain reaction (qPCR) (fig. S2, A and C). To test the impact of these RBPs on circRNA biogenesis, we selected five MB expressed circRNAs (circMTDH, circCACNA2D1, circFIP1L1, circHNRNPM, circRBM28) that harbor the binding sites for all four RBPs in the intronic regions flanking the BSJ (Fig. 2, B to F; fig. S2, D to H; and table S7). Strikingly, we observed that knockdown of hnRNP C was sufficient to significantly induce the expression of all five circRNAs in group 3 MB cells. Notably, increased circRNA expression was also accompanied by the concomitant reduction of the cognate linear transcript in D341 cells (Fig. 2, B to E), indicating that hnRNP C may modulate the competition between back- and linear splicing in these target genes. By contrast, the knockdown of the other three RBPs caused only mild or no effects on the expression of these circRNAs (Fig. 2, B to F, and fig. S2, D to H). The same effect of hnRNP C knockdown was observed by using two different small interfering RNAs (siRNAs) in both cell lines (Fig. 2A and fig. S2B), except for circCACNA2D1 that was only significantly up-regulated in D341 cells (Fig. 2C). Together, these results suggest that hnRNP C plays a functional role in the negative regulation of circRNA biogenesis in group 3 MB cells.

To further explore the functional role of hnRNP C as general repressor of circRNA biogenesis, we carried out RNA-seq analyses in D341 cells. Treatment of the RNA samples with ribonuclease R (RNase R) (fig. S3, A and B) was performed to enrich for circRNAs while removing linear RNAs (*31*). Principal components analysis (PCA) and unsupervised clustering of RNAse R-treated cells confirmed the segregation of control and hnRNP C–depleted samples (fig. S3C). The analysis of RNase R-treated samples by the CIRI software identified a total of 19,291 BSJs in D341 cells (table S8). In agreement with previous findings (*5*), introns flanking the exons undergoing back-splicing in D341 cells are longer and contain more inverted and repeated

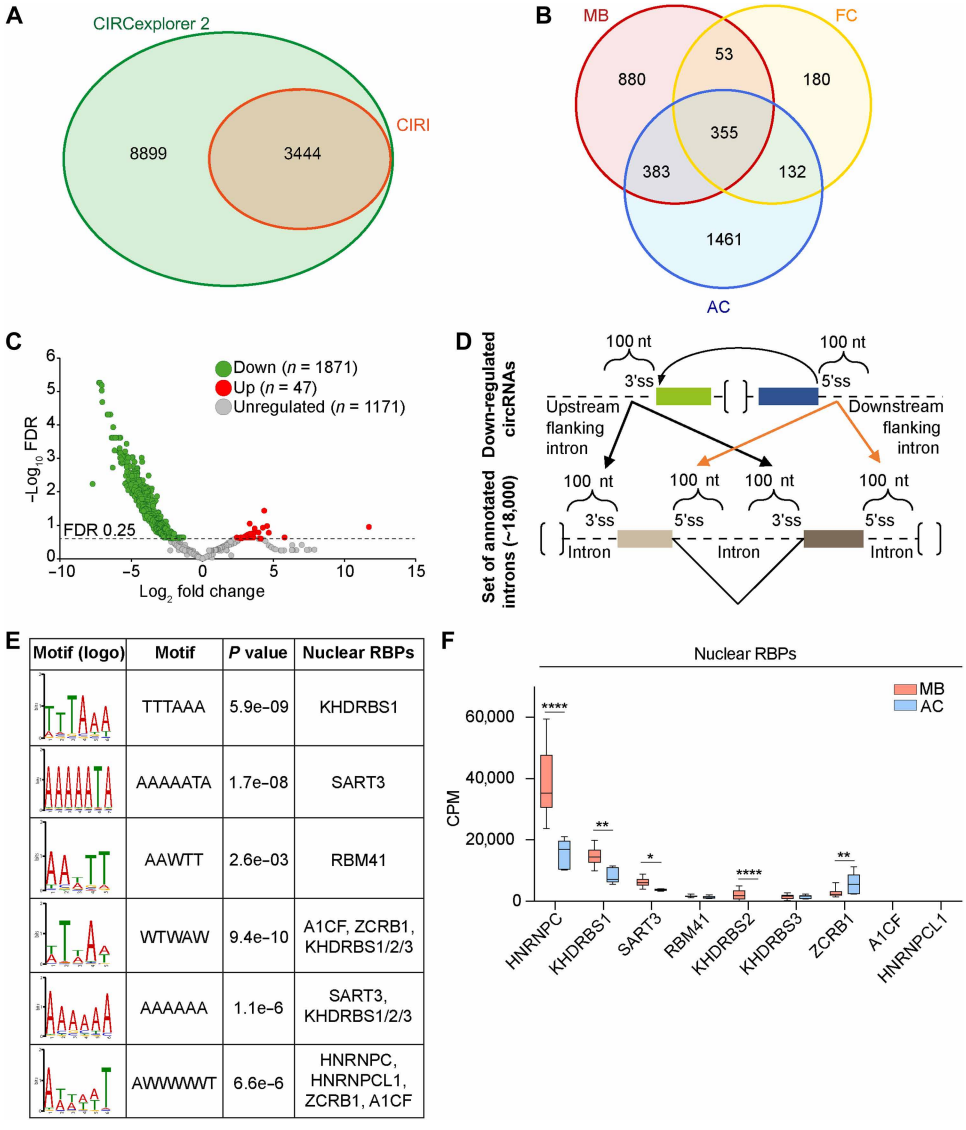

Fig. 1. CircRNA expression is extensively down-regulated in patients with group 3 MB. (**A**) Identification of circRNAs querying EGAD00001004958 RNA-seq dataset. Venn diagram showing the intersection between CircExplorer2 and CIRI ($n = 3444$) computational analysis. (**B**) Venn diagram depicting the number of circRNAs identified in healthy cerebella (AC, $n = 5$; FC, $n = 4$) and group 3 MB (MB, $n = 16$). (**C**) Differential expression analysis of circRNAs detected in group 3 MB and adult cerebellum (AC). circRNAs differentially expressed (FDR < 0.25) were highlighted in red and green. (**D**) Scheme depicting the strategy for the motif enrichment analysis using STREME-TomTom (MEME suite; https://meme-suite.org/meme/) in circRNAs flanking introns. (**E**) Motifs and corresponding RBPs predicted in motif enrichment analysis in (D). (**F**) mRNA expression levels (cpm, count per million reads) in EGAD00001004958 RNA-seq data of nuclear RBPs whose binding sites were enriched (Benjamini-Hochberg adjusted *P* values; **P* < 0.05, ***P* < 0.01, and *****P* < 0.0001).

Alu (IR*Alu*) elements than introns not surrounding circularization events (fig. S3, D and E, and tables S9 and S10). Notably, introns flanking BSJs were also enriched for stretches of ≥9 uridine residues (fig. S3F and table S11), which are strong binding motifs for hnRNP C (*32*). To directly determine the role of hnRNP C on circRNA biogenesis, we then focused on 3479 high-confidence back-splicing events from 2050 genes that showed at least two read counts in at least two replicates of either control (siNC) or hnRNP C–depleted (siHNRNPC) D341 cells (table S8). The vast majority (94.7%) of these back-splicing events involved exons (Fig. 3A and table S8). Notably, the knockdown of hnRNP C induced a robust increase in the number of unique BSJs (~4-fold; Fig. 3B) and in circRNA-producing genes (3.5-fold; Fig. 3C). Furthermore, the comparison of back-splicing and linear splicing in transcripts expressed in all samples ($n = 1685$; table S8) showed a highly significant increase of circRNA:linear RNA ratio in hnRNP C–depleted cells (Fig. 3D), suggesting that hnRNP C modulates the balance between linear and circular splicing in these cells. Moreover, transcriptome analyses of parallel samples not treated with RNAse R indicated that the depletion of hnRNPC has a significantly stronger impact on the modulation of circRNAs (17% of expressed genes) than on canonical splicing (6%) and gene expression (5%) (Fig. 3E, fig. S3G, and tables S12 and S13).

Our analysis indicated that depletion of hnRNP C affects 376 circRNAs in D341 cells, with ~90% of them being up-regulated (Fig. 3F

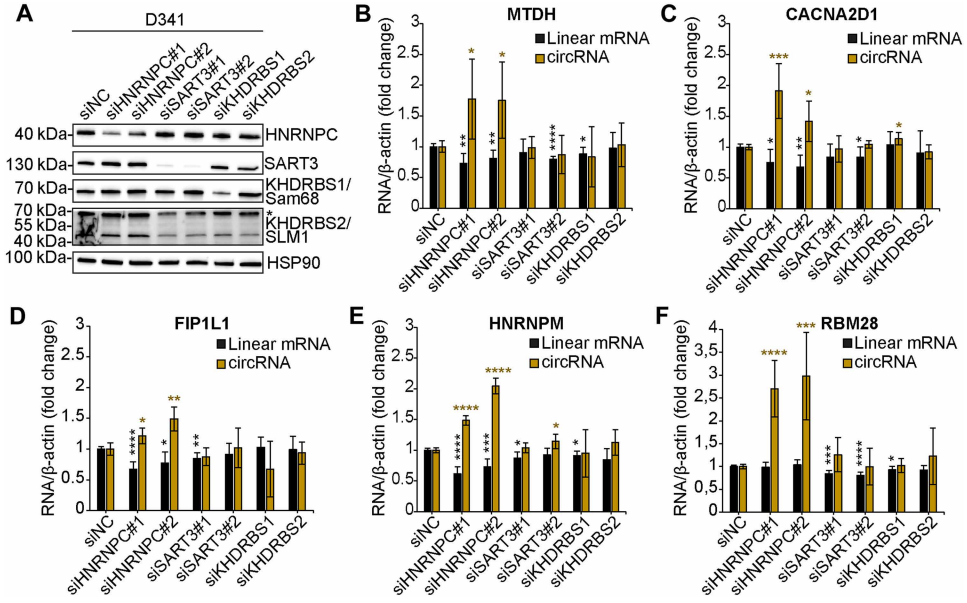

Fig. 2. HnRNP C represses the expression of circRNAs in group 3 MB cells. (**A**) Western blot analysis evaluating the expression of the selected RBPs upon their silencing in D341 cells. Asterisk (*) indicates a not-specific signal for KHDRBS1/Sam68 in KHDRBS2/SLM1 Western blot. (**B** to **F**) RT-qPCRs detecting parental linear mRNAs and circRNAs having enrichment for HNRNPC, SART3, and KHDRBS1/2 binding sites in the flanking introns. #1 and #2 indicate two different siRNAs. siNC: siRNA negative control ($n = 3$; means ± SD; Student's t test versus siNC; $^{*}P < 0.05$, $^{**}P < 0.01$, $^{***}P < 0.001$, and $^{****}P < 0.0001$).

and tables S8 and S14). Notably, the analysis of the genes generating the up-regulated circRNAs ($n = 311$) by the Molecular Signatures Database (MSigDB) uncovered an enrichment in MYC target and mitotic spindle genes (Fig. 3G, top). Furthermore, Gene Ontology analyses highlighted a significant enrichment in genes associated with chromatin remodeling and positive regulation of DNA repair (Fig. 3G, bottom), two biological processes involved in tumor evolution and resistance to chemotherapy. Together, these findings suggest that hnRNP C is required to repress excessive circularization of transcripts that are crucial for group 3 MB cell viability and proliferation. Analysis by reverse transcription–qPCR (RT-qPCR) validated the increased expression of five of six and six of six of the up-regulated circRNAs in, respectively, D341 and HD-MB03 cells (Fig. 3H, fig. S3H, and table S14).

Introns flanking circularizing exons are enriched in strong binding sites for hnRNP C in close proximity of *Alu* elements

Analyses of sequence features indicated that introns flanking hnRNP C–repressed BSJs are shorter (Fig. 4A and tables S8 and S15) and characterized by increased frequency of IR*Alu* elements and of hnRNP C–binding sites with respect to introns surrounding unregulated back-splicing events (Fig. 4, B and C, and tables S8, S15, and S16). Moreover, the hnRNP C–binding sites are found at the beginning of intronic *Alu* elements, regardless of regulation, but they are closer to the regulated BSJs than the nonregulated ones (Fig. 4, D and E, and tables S17 and S18). Thus, hnRNP C preferentially represses back-splicing events mediated by introns with IR*Alu* close to the splice sites.

To evaluate whether hnRNP C may directly bind in proximity of *Alu* elements at genome-wide level, we analyzed ultraviolet (UV) crosslinking and immunoprecipitation sequencing (iCLIP-seq) data (*33*). We found that 33.82% ($n = 148,248$) of hnRNP C peaks are associated with *Alu* elements [Alu sequence +15 base pair (bp) on each side]. Among them, 35.07% ($n = 51,985$) of these binding sites are in intronic *Alu* elements flanking the detected BSJs (tables S19 and S20 and fig. S4, A and B). The 64.37% ($n = 215$ of 344) of up-regulated BSJs showed iCLIP peaks of hnRNP C in the flanking introns (Fig. 4F and table S21). Together, these data support a direct impact of hnRNP C on circRNA biogenesis through binding in proximity of inverted *Alu* elements in the introns flanking the BSJ. To validate this hypothesis in the MB context, we performed CLIP-qPCR experiments. Strikingly, the strong binding of hnRNP C was observed in close proximity of *Alu* elements within the introns flanking the regulated BSJs, where its binding sites were predicted to be located (Fig. 4, G and H). Thus, hnRNP C acts as general repressor of circRNA biogenesis in group 3 MB cells through direct binding to *Alu* elements.

Binding of hnRNP C is necessary to inhibit back-splicing events

We hypothesized that hnRNP C binding at the beginning of the *Alu* elements may interfere with IR*Alu* pairing between the introns flanking circularizing exons, thus repressing circRNA biogenesis. To test this hypothesis, we took advantage of an *Survival Motor Neuron 2* (*SMN2*) circRNA-producing minigene previously validated in our laboratory (*7*). First, we observed that hnRNP C depletion caused the up-regulation of the endogenous circSMN9-6 in D341 cells (Fig. 5A). Next, we used the *SMN2* minigene encompassing the coding region of the *SMN2* gene from exon 5 to the region downstream of exon 8, which comprises the cryptic exon 9 involved in the back-splicing event with exon 6 (*7*). An internal portion of intron 6 was deleted to reduce the size of the minigene, while a six-nucleotide TAG was inserted in exon 6 to allow discrimination of the recombinant RNA products from endogenous transcripts (Fig. 5B). *SMN2* intron 5, which represents the upstream intron involved in the back-splicing event, has all the sequence features highlighted by our bioinformatics analysis (Fig. 4, A to E). First, it is a relatively small intron (1310 bp) comprising two *Alu*

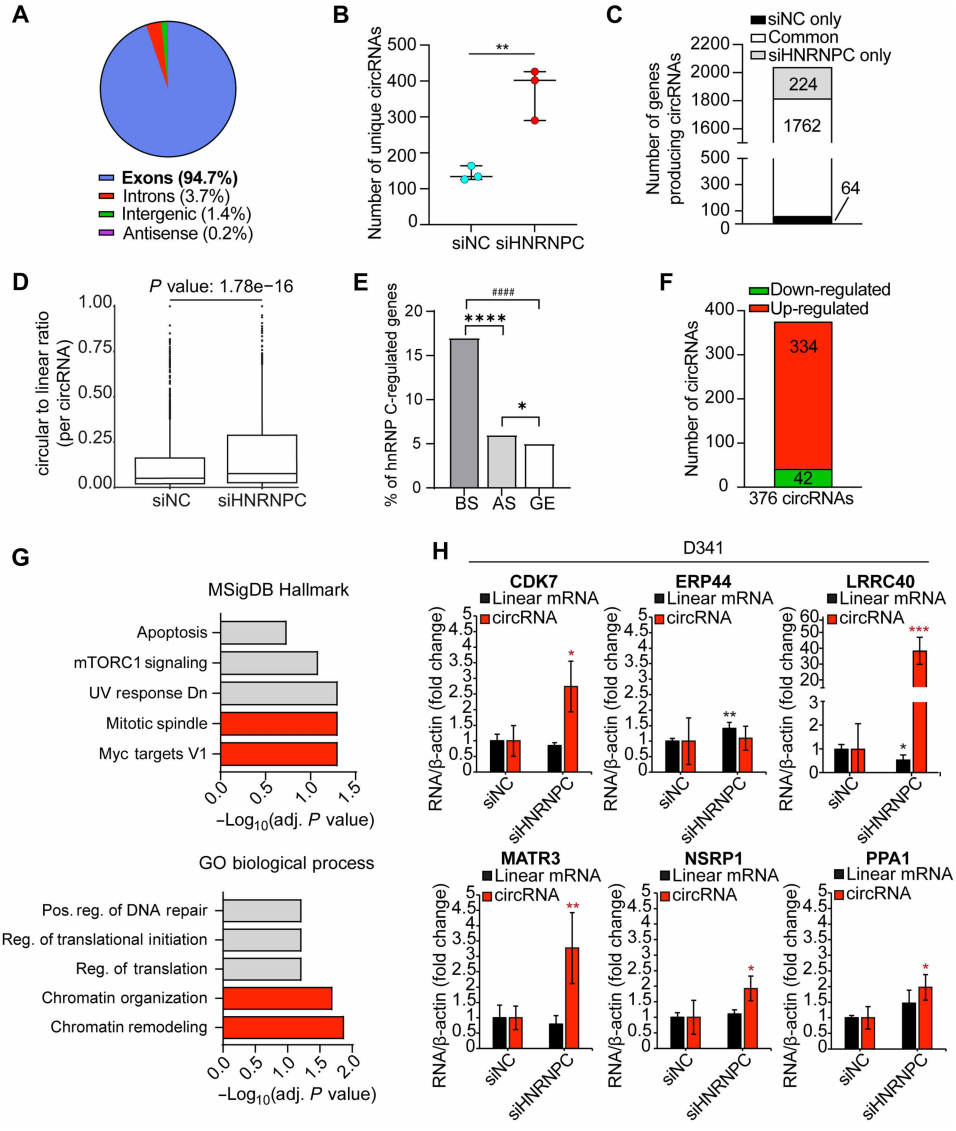

Fig. 3. HnRNP C is a general repressor of circRNA biogenesis in group 3 MB cells. (**A**) Percentage of circRNAs generated from exons, introns, intergenic regions, and antisense transcripts in siNC and siHNRNPC samples. (**B**) Number of unique circRNAs detected in siNC- and siHNRNPC-treated D341 cells. Median with interquartile range is shown (Student's *t* test; $^{**}P < 0.01$). (**C**) Number of circRNA-producing genes in siNC and siHNRNPC samples. (**D**) Circular to linear read-count ratio per circRNA in control and HNRNPC-depleted cells. *P* value is shown (Student's *t* test). (**E**) Percentage of hnRNP C–regulated genes in terms of back-splicing (BS; $n = 352$), alternative splicing (AS; $n = 648$), and gene expression (GE; $n = 572$). Fisher's exact test; $^{*}P = 0.03$, $^{****}P = 8.17 \times 10^{-51}$, and $^{\#\#\#\#}P = 6.5 \times 10^{-60}$. (**F**) Number of up-regulated and down-regulated circRNAs upon HNRNPC depletion. (**G**) Gene set enrichment analysis of the genes generating up-regulated circRNAs was performed using Enrichr (https://maayanlab.cloud/Enrichr/). (**H**) Validation of six up-regulated exonic circRNAs contained in the list of the top 8 most up-regulated circRNAs in HNRNPC-depleted cells ($n = 4$; means ± SD; Student's *t* test versus siNC; $^{*}P < 0.05$, $^{**}P < 0.01$, and $^{***}P < 0.001$).

elements (AluSq; +364 to 671 bp and FLAM_C; +1051 to 1188 bp) and two strong binding sites for hnRNP C located at nucleotide +374 [binding site 1 (BS1); stretch of 13 uridine residues] and + 879 [binding site 2 (BS2); stretch of 12 uridine residues]. Both hnRNP C–binding sites are located at the beginning of the *Alu* elements. Furthermore, BS2 is relatively close (420 bp) to the acceptor back-splicing site (Fig. 5B). The transfection of the minigene in human embryonic kidney (HEK) 293T cells resulted in the production of the expected circSMN9-6 (Fig. 5C). The hnRNP C depletion strongly increased the expression of circSMN9-6 (Fig. 5C), indicating that this minigene is suitable to study the hnRNP C–dependent regulation of circRNA biogenesis. To test whether binding of hnRNP C near the *Alu* elements is required to repress circRNA biogenesis, we mutagenized the minigene to disrupt the hnRNP C binding sites. To this aim, we replaced both binding sites for hnRNP C in intron 5, alone or in combination, by substituting the thymidine stretch with adenines (Fig. 5D and fig. S4C). Strikingly, the mutation of either hnRNP C–binding site increased circSMN9-6, with BS1 showing a stronger effect. Moreover, the combined disruption of both binding sites completely rescued circRNA biogenesis to the same levels of hnRNP C silencing (Fig. 5E). These results suggest that hnRNP C binding in proximity of *Alu* elements is necessary and sufficient to repress the SMN circRNA biogenesis.

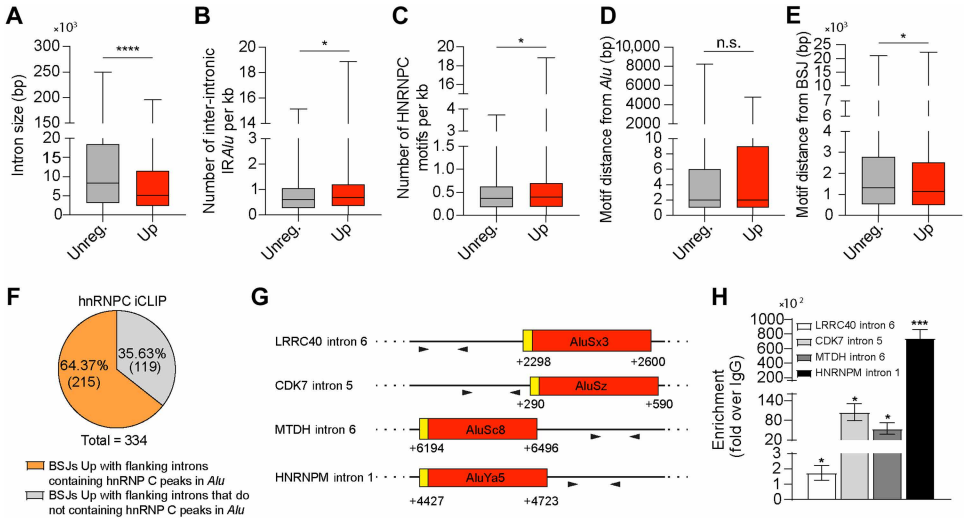

Fig. 4. Introns flanking circularizing exons are enriched for hnRNP C strong binding sites in proximity of *Alu* elements. (**A** to **E**) Features of the flanking introns sequences belonging to the up-regulated circRNAs in HNRNPC-depleted cells compared to flanking introns of unregulated circRNAs. Student's *t* test; $*P < 0.05$ and $****P < 0.0001$; n.s., not significant. (**F**) Pie chart showing the percentages and numbers of BSJs up-regulated by hnRNP C and characterized by flanking introns containing hnRNP C iCLIP peaks in *Alu* elements. (**G**) Schematic representation of hnRNP C–binding sites analyzed by CLIP-qPCR within the indicated transcripts. Yellow boxes indicate predicted hnRNP C–binding motifs overlapping with *Alu* elements (shown in red). Arrowheads denote the positions of primer pairs used in CLIP-qPCR to quantify pre-mRNA region bound by hnRNP C. Nucleotide positions are given relative to the intron start site, where the first nucleotide of the intron is designated as +1. (**H**) CLIP assays performed in D341 cells using anti-hnRNP C antibody or IgGs as a negative control. Data are represented as fold change enrichment over IgGs ($n = 3$; means ± SEM; Student's *t* test versus IgG; $*P < 0.05$ and $***P < 0.001$).

HnRNP C represses the accumulation of intron-derived dsRNAs and spurious activation of innate immune response in group 3 MB cells

The main mechanism underlying the regulation of circRNA biogenesis is the pairing of intronic IR*Alu* elements (*5*). We reasoned that these structures, if not properly controlled, may generate stable dsRNA adducts that could accumulate in the cell. To test this hypothesis, we carried out immunofluorescence assays with the J2 antibody, which specifically recognizes dsRNAs, in hnRNP C–depleted HD-MB03 cells, which grow in adherence and are more suitable for immunofluorescence analyses. Quantitative analysis of fluorescence intensity indicated that depletion of hnRNP C significantly increases the accumulation of cytoplasmic dsRNAs (Fig. 6, A and B). The effect of hnRNP C knockdown on the accumulation of dsRNAs was similar to that elicited by DHX9 knockdown, a DNA/RNA helicase previously shown to globally inhibiting circRNA biogenesis by resolving the pairing of IR*Alu*-rich intronic regions and to repress cytosolic dsRNA accumulation (*34*).

To test whether intron flanking the hnRNP C–regulated BSJs contributed to this dsRNA accumulation, we performed subcellular fractionation assays in control and hnRNP C–depleted group 3 MB cells (fig. S5A). RT-qPCR analysis using primers in proximity to *Alu* sequences of introns flanking 4 arbitrarily selected BSJs revealed the accumulation of these introns in the cytoplasmic fractions of hnRNP C–depleted cells (fig. S5B). The treatment of the extracts with RNase III, an endonuclease that degrade dsRNAs while preserving single strand RNAs (*35*), significantly reduced the accumulation of these intronic sequences in the cytoplasm (fig. S5B). This observation suggests that these BJS-flanking introns are organized as cytoplasmic dsRNAs. To further corroborate this hypothesis, we immunoprecipitated cytoplasmic dsRNAs from control and hnRNP C–depleted cells by using the dsRNA-specific J2 antibody. Consistent with our hypothesis, we observed introns flanking the BSJs in the J2 immunoprecipitate, indicating that they can form stable dsRNA molecules. Moreover, we detected a significant increase of these introns in the dsRNA samples isolated from cells depleted for hnRNP C (Fig. 6C). Introns flanking a non-regulated BSJ were also detected among the J2-immunoprecipitated dsRNAs. However, their abundance in the cytoplasm was not modulated upon hnRNP C depletion (fig. S5C). These data indicate that the increased circularization caused by hnRNP C depletion is associated with increased formation of cytoplasmic dsRNAs.

To more directly test the contribution of circRNA biogenesis to the accumulation of cytoplasmic dsRNAs, we exploited the *SMN2* minigene, which contains a sequence TAG that allows discrimination of transcripts generated by this recombinant construct from endogenous RNAs (Fig. 5). HEK293T cells were transfected with *SMN2* wild-type (WT) or BS1 minigene, and we measured circRNA, intron retention (IR)—as a possible RNA processing defect from which dsRNAs can be generated—and cytoplasmic dsRNA levels in the recipient cells. We found that the increased expression of circSMN9-6 derived from the BS1 mutant minigene (Fig. 6D) was associated with increased cytoplasmic accumulation of dsRNAs, which were isolated with the J2 antibody and detected by primers in either intron 5 or intron 9 that flank the BSJ (Fig. 6F). On the other hand, no significant increase in intron retention (IR) was detected from this mutant minigene (Fig. 6E). Next, to further test the relative contribution of circRNA biogenesis and altered RNA processing to the accumulation of dsRNAs, we treated HEK293T cells transfected with the WT minigene with either hnRNP C siRNAs or pladienolide B (PdB), a splicing inhibitor that causes pervasive IR (*36*, *37*). Under these conditions, we found that depletion of hnRNP C induced a strong up-regulation of the circSMN9-6 with minimal effect on retention of intron 5 (intron upstream of the

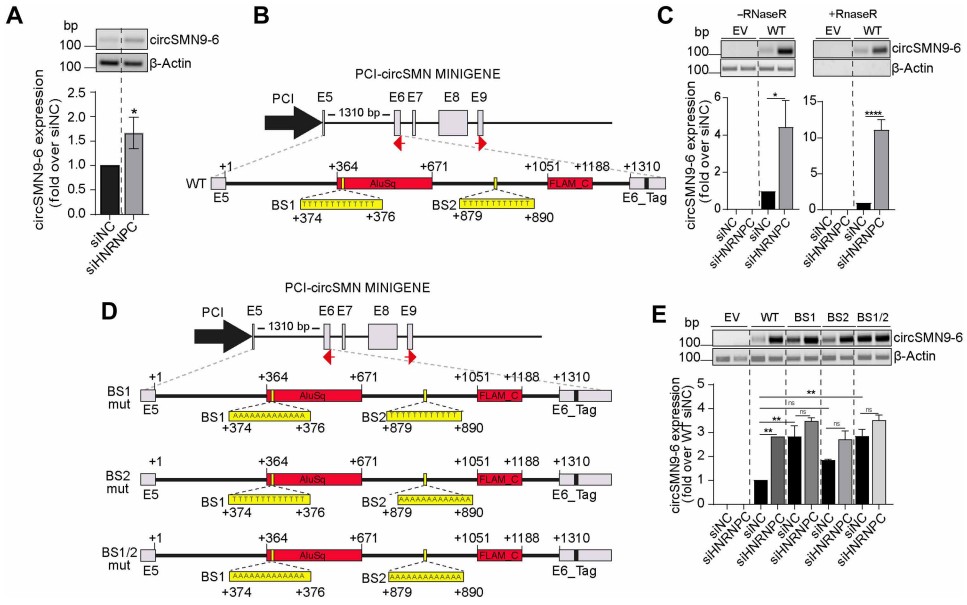

Fig. 5. Binding of hnRNP C is necessary to inhibit back-splicing events. (**A**) Representative RT-PCR image (top) and densitometric analysis (bottom) showing endogenous circSMN9-6 expression in D341 cells transfected with siNC or siHNRNPC. Actin was used as a loading control ($n = 3$; means ± SD; Student's t test; $P \leq 0.05$). (**B**) Schematic representation of the wild-type circSMN9-6 minigene (WT). Gray boxes indicate exons, red boxes represent *Alu* elements, black lines denote introns, and red arrows indicate divergent primers used for the detection of minigene-derived circSMN9-6. The nucleotide sequence highlights HNRNPC-binding sites within SMN2 intron 5. (**C**) Representative RT-PCR image (top) and densitometric analysis (bottom) showing minigene-derived circSMN9-6 expression in HEK293T cells transfected with either empty vector (EV) or the circSMN9-6 WT minigene, with or without RNase R treatment. Actin was used to normalize RNA input ($n = 3$; mean ± SD; one-way ANOVA; $^*P < 0.05$ and $^{****}P < 0.0001$). (**D**) Schematic representation of mutant circSMN9-6 minigenes. BS1, BS2, and BS1/BS2 indicate mutations in HNRNPC-binding site 1, HNRNPC-binding site 2, and both sites, respectively. (**E**) Representative RT-PCR image (top) and densitometric analysis (bottom) showing circSMN9-6 expression derived from mutant minigenes in HEK293T cells transfected with BS1, BS2, or BS1/BS2 constructs, following transfection with siNC or siHNRNPC. Actin was used as a loading control ($n = 3$; means ± SD; Student's t test; $^{**}P < 0.01$).

BSJ). By contrast, PdB caused strong IR without promoting circularization of the transcript (Fig. 6, G and H). Thus, this experimental setting allows us to investigate the relative contribution of circRNA biogenesis and IR to the accumulation of dsRNAs. We then immunoprecipitated cytoplasmic dsRNAs with the J2 antibody from all samples. Our results indicate that cytoplasmic dsRNAs are significantly induced by silencing of hnRNP C, but not by PdB, which only induces a mild and not significant increase with respect to untreated cells (Fig. 6I). Together, these data support the notion that introns involved in circRNA biogenesis significantly contribute to the accumulation of cytoplasmic dsRNAs in hnRNP C–depleted cells, independently from intron-retaining transcripts generated by altered linear splicing (e.g., PdB). These findings uncover a previously unknown source of cytoplasmic dsRNAs as by-products of excessive circRNA biogenesis and a key role on hnRNP C in preventing the accumulation of these nucleic acids adducts.

The accumulation of cytoplasmic dsRNAs in hnRNP C–depleted HD-MB03 cells positively correlated with the up-regulation of interferon-stimulated genes (ISGs) (i.e., TNF, IFNB1, CXCL10, IFI27, and IFI44; Fig. 7A). Unexpectedly, DHX9 depletion increased the expression of only two ISGs among those tested (CXCL10 and IFI44), suggesting that, at least in HD-MB03 cells, hnRNP C depletion triggers a stronger interferon response than DHX9 (Fig. 7A). IFNB1, IFI27, and IFI44 up-regulation was observed also in D341 cell (fig. S5, D and E). Accordingly, hnRNP C depletion impaired cell viability in D341 and HD-MB03 cell lines (Fig. 7, B and C) and reduced MB spheroid formation in D341 cells (Fig. 7, D and E).

Together, these results highlight a previously unexplored role for hnRNP C as general repressor of IR*Alu* pairing and pre-mRNA circularization, which contributes to the safeguard of the human transcriptome integrity and to control inappropriate activation of the innate immune response.

DISCUSSION

CircRNA expression is strongly inhibited in cancer cells with respect to healthy tissues (*11*, *12*). CircRNAs are generally more stable than linear transcripts and tend to accumulate in long-lived and postmitotic cells, such as neurons. At the same time, however, circRNA biogenesis has lower efficiency than production of canonical mRNAs through linear splicing (*1*). Thus, the lower content of circRNAs in cancer cells might represent the consequence of their higher proliferation rate and dilution of these less efficiently produced transcripts. However, mounting evidence also suggest that the inhibition of circRNA biogenesis is important to sustain proliferation and viability of tumor cells (*4*). Here, we identify hnRNP C as an important negative regulator of circRNA biogenesis in group 3 MB. First, we observed a strong down-regulation of circRNA expression in samples from patients with group 3 MB compared to adult healthy cerebellum. A limitation of this analysis consists in the analysis of publicly available polyadenylate [poly(A)]–enriched libraries, which might lead to an underestimation of circRNA expression. Nevertheless, since we performed the comparative analysis of MB, normal fetal and normal adult cerebella datasets that were all generated by

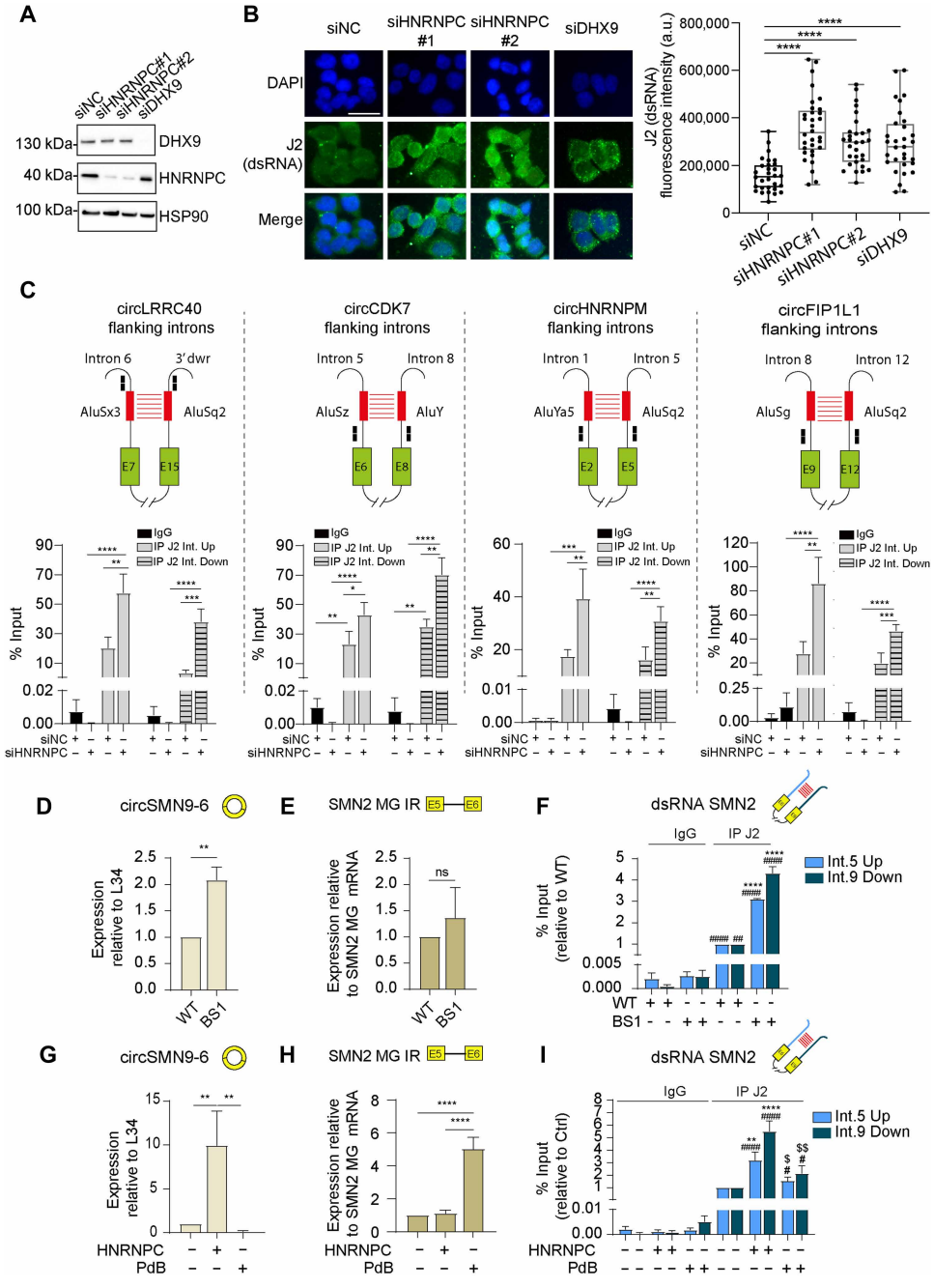

Fig. 6. HnRNP C represses the accumulation of intron-derived dsRNAs. (**A**) WB of HD-MB03 transfected as indicated. (**B**) IF of dsRNA in HD-MB03 treated as above. Scale bar, 20 μm. Right panel shows quantification of cytoplasmic dsRNA signal ($n = 3$; Student's t test versus siNC). (**C**) RT-qPCR showing the enrichment of introns flanking the selected hnRNP C–regulated BSJs in the J2-immunoprecipitated (IP J2) fractions from cytosolic RNA of hnRNP C–depleted HD-MB03 ($n = 4/7$; means ± SEM; two-way ANOVA). Int. Up and Int. Down stand for upstream and downstream introns, respectively. The top panel shows a schematic representation of the introns. Green boxes represent exons, and black lines represent introns. Red boxes indicate *Alu* elements. Black boxes show primer pairs used. (**D**) RT-qPCR of minigene-derived circSMN9-6 in WT or BS1 minigene-transfected HEK293T. WT was set to 1 ($n = 3$; means ± SEM; Student's t test). (**E**) RT-qPCR of minigene-derived intron 5 retention in HEK293T, as above ($n = 3$; means ± SEM; Student's t test). (**F**) RT-qPCR showing the enrichment of SMN2 intron 5 and 9 in cytosolic fraction of HEK293T, as above (n = 3; means ± SEM; one-way ANOVA; #IP J2 versus IgG; *BS1 versus WT). (**G**) RT-qPCR of minigene-derived circSMN9-6 in HEK293T transfected with WT minigene and treated with sihnRNP C or PdB. Control was set to 1 ($n = 3$; means ± SEM; one-way ANOVA). (**H**) RT-qPCR of minigene-derived intron 5 retention in HEK293T, as above ($n = 3$; means ± SEM; one-way ANOVA). (**I**) RT-qPCR showing the enrichment of SMN2 intron 5 and 9 in cytosolic fraction of HEK293T, as above ($n = 3$; means ± SEM; one-way ANOVA; #IP J2 versus IgG; *, sihnRNP C– or PdB-treated samples versus WT; $, sihnRNP C versus PdB). * or # or $$P < 0.05$; ** or ## or $$P < 0.01$; ***$P < 0.001$; and **** or ####$P < 0.0001$). DAPI, 4′,6-diamidino-2-phenylindole.

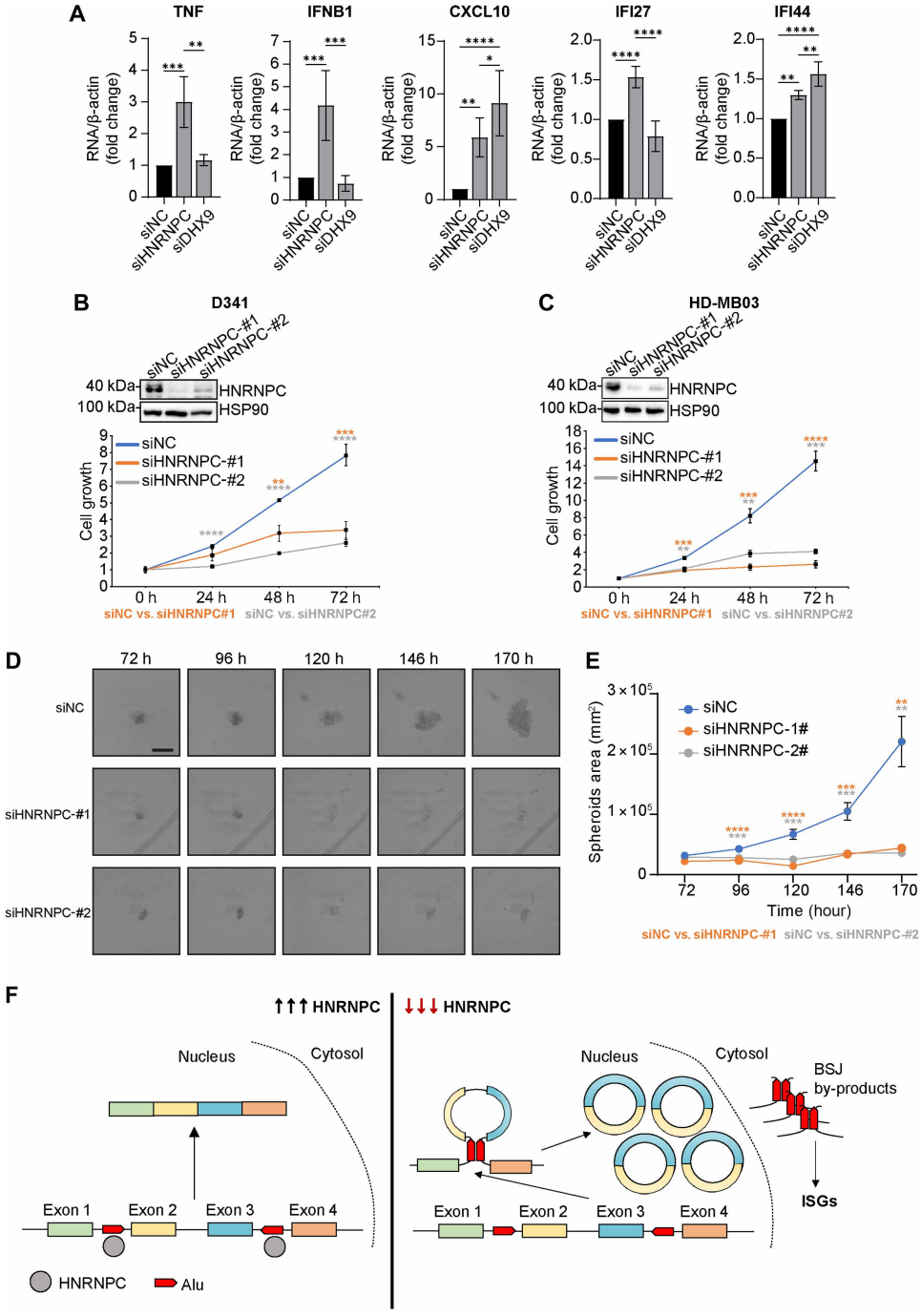

Fig. 7. HnRNP C represses the spurious activation of innate immune response in group 3 MB cells. (**A**) RT-qPCR analysis of immune-related genes in HD-MB03 cells treated with the indicated siRNAs ($n = 3$; means ± SD; one-way ANOVA, $^{*}P < 0.05$, $^{**}P < 0.01$, $^{***}P < 0.001$, and $^{****}P < 0.0001$). (**B**) Cell growth analysis in D341 cells transfected with the indicated siRNAs ($n = 3$; Student's t test versus siNC; $^{*}P < 0.05$, $^{**}P < 0.01$, $^{***}P < 0.001$, and $^{****}P < 0.0001$). (**C**) Cell growth analysis in HD-MB03 cells transfected with the indicated siRNAs ($n = 3$; means ± SD; Student's t test versus siNC; $^{*}P < 0.05$, $^{**}P < 0.01$, $^{***}P < 0.001$, and $^{****}P < 0.0001$). (**D**) Microscope images of D341 spheroids at the indicated time points after seeding. Scale bar, 500 μm. (**E**) Quantification of spheroids area at the indicated time points ($n = 12$; means ± SEM; Student's t test versus siNC; $^{*}P < 0.05$, $^{**}P < 0.01$, $^{***}P < 0.001$, and $^{****}P < 0.0001$). (**F**) Schematic model showing the suppressive role of HNRNPC on circRNA expression in group 3 MB, preventing the accumulation of cytoplasmic dsRNAs. ISGs, interferon-stimulated genes.

poly(A)-enriched libraries, this issue does not introduce a bias in the identification of the differentially expressed circRNAs.

CircRNA down-regulation in group 3 MB samples correlated with the higher expression levels of hnRNP C. By contrast, fetal healthy cerebellum, which express comparable levels of hnRNP C (fig. S1C), also expressed low levels of circRNAs, supporting a role for this RBP in the regulation of circRNA biogenesis in the healthy and pathological cerebellum. Moreover, we found that the depletion of hnRNP C expression in group 3 MB cells strongly increases the expression of hundreds of circRNAs, supporting the role of this RBP as a general repressor of circRNA biogenesis. These observations suggest that proliferative nervous tissues, such as fetal cerebellar precursor cells and MB cells, are more dependent on linear splicing for the production of large amounts of mRNAs and require high expression of hnRNP C to modulate the balance in favor of canonical splicing. This scenario might be particularly relevant for MYC-amplified group 3 MB due to the MYC-dependent transcriptional overload and the consequent higher dependence on an efficient splicing machinery for guaranteeing cell viability (*16*). Notably, another recurrent aberration in group 3 MB is the amplification of the oncogenic transcription factor OTX2 (*13*), which was shown to induce the expression of hnRNP C (*38*). OTX2 physically interacts with hnRNP C and other members of the large assembly of splicing regulators complex to drive an AS program that is essential to maintenance of stemness potential and progression of group 3 MB (*38*). This experimental evidence further supports the strong dependence of MYC- and/or OTX2-amplified group 3 MB from canonical splicing. In this sense, hnRNP C might function both to execute a cancer-related splicing program and, concomitantly, to prevent the usage of splice sites in noncanonical events, such as back-splicing.

Our unbiased search for RNA binding motifs enriched in the introns flanking the regulated BSJs has identified hnRNP C, KHDRBS1/Sam68, SART3, and KHDRBS2/SLM1 as potential regulator of circRNA biogenesis in group 3 MB cells. All four RBPs were highly expressed in patients with group 3 MB at transcript and protein level. However, only hnRNP C depletion affected on circRNA biogenesis. Previous data indicated the possible implication of hnRNP C as regulator of pre-mRNA circularization. In particular, hnRNP C was shown to regulate the expression of three hypoxia-regulated circRNAs (circCDYL2, circRARS, and circSMARCA5) in HeLa cells, with two of them being repressed and one promoted by this RBP (*30*). However, to our knowledge, our study shows for the first time that hnRNP C acts as a general regulator of circRNA biogenesis with possible functional implications in MB context. For some pre-mRNA targets, we show that hnRNP C depletion cause a concomitant increase in circularization and decrease in the linear counterpart, pointing to a key role of this RBP in the well-known competition between the canonical linear splicing and back-splicing (*21*–*23*). We posit that hnRNP C might function by repressing the formation of IR*Alu*-mediated secondary structures in the pre-mRNA that are necessary to promote noncolinear splicing, thus ensuring linear processing of transcripts. This hypothesis is supported by our bioinformatics analyses showing that the circularization index—the relative abundance of circRNA versus spliced linear mRNA—is significantly higher in hnRNP C–depleted cells, highlighting their higher proficiency to promote back-splicing of nascent pre-mRNAs. This role of hnRNP C as general repressor of circRNA biogenesis might be particularly relevant for group 3 MB, which is frequently driven by oncogenic transcriptional factors (MYC and OTX2) that increase the transcriptional rate of the cell and may favor the prolonged life of intron-retaining transcripts, due to increased competition between introns for the splicing machinery. The role of hnRNP C as repressor of IR*Alu*-mediated back-splicing is in line with its previously proposed role as repressor of cryptic intronic splice sites and exonization of transposable elements (*33*). Thus, hnRNP C may play a general role as guardian of the integrity of the human transcriptome by preventing aberrant exon inclusion and/or excessive circularization of pre-mRNAs comprising high density of transposable elements. Moreover, since genes affected by pre-mRNA circularization are enriched in terms of high relevance for group 3 MB, such as MYC targets, mitotic spindle, chromatin remodeling, and DNA repair (*39*), the high expression of hnRNP C is likely required to favor linear splicing of transcripts that support oncogenic features of group 3 MB cells.

Our bioinformatics analyses of RNAse R-treated group 3 MB cells showed that the number of circRNAs and circRNA-generating genes was strongly increased in hnRNP C–depleted cells. The impact of hnRNP C depletion on circRNA expression (17% of total) was significantly broader than on canonical splicing (6% of total) or gene expression (5% of total). Furthermore, ~90% of these circRNAs were up-regulated in the absence of hnRNP C. The introns flanking the regulated BSJs are significantly smaller and, more importantly, enriched for inter-intronic IR*Alu* and hnRNP C–binding sites. Given that hnRNP C preferentially binds *Alu* elements (*33*), the higher number of hnRNP C–binding motifs in introns flanking BSJs might be due to the higher concentration of inter-intronic IR*Alu*. However, the hnRNP C–binding motifs are closer to the up-regulated BSJs than to the unregulated BSJs. Thus, it is likely that hnRNP C represses the circularization of transcripts that, due to their intrinsic sequence features, tend to form IR*Alu*-mediated dsRNAs near a BSJ. Structurally, although hnRNP C contains only one RNA recognition motif, it oligomerizes into tetramers to form a complete functional unit for RNA binding (*32*). In line with this notion, "strong" binding motifs for hnRNP C comprise stretches of ≥9 uridines (*32*). Coherently, we found these strong hnRNP C–binding motifs at the beginning of *Alu* elements in both unregulated and regulated BSJs, which probably coincides with the terminal poly(A) tail of the *Alu* element at the time of its insertion into the genome in opposite orientation. Previous experimental evidence showed the preferential binding of hnRNP C to antisense *Alu* elements (*33*). Furthermore, our in vitro mutagenesis experiments showed that mutation of the U-stretch in the predicted binding site for hnRNP C strongly increased the circularization of the circSMN2(ex9-6) and mimicked the effect of hnRNP C depletion. These results suggest that the direct binding of hnRNP C to U-stretches in proximity of IR*Alu* elements is required to repress the circularization of target transcripts. However, it is also conceivable that monomeric hnRNP C binds with lower affinity to shorter U-stretches along the entire length of *Alu* elements, thus contributing to further repress their pairing.

Our results also show that introns flanking hnRNP C–regulated BSJs accumulate into the cytoplasm as dsRNAs, thus activating the innate immune response. Since treatment with RNAse III completely abrogated their cytoplasmic accumulation, these RNA sequences from introns flanking the hnRNP C–regulated BSJs are likely structured in dsRNAs. In support of these data, we found a significant accumulation of introns flanking the up-regulated BSJs in the J2-immunoprecipitated cytoplasmic fraction upon hnRNP C depletion. Thus, we hypothesize that dsRNAs generated by BSJ-flanking introns are by-products of the increased circRNA biogenesis, which leak out into the cytoplasm

and activate an innate immune response that hampers viability and proliferation of group 3 MB–depleted cells. In this scenario, the high expression of hnRNP C is required to maintain circRNA biogenesis under control and to limit the accumulation of dsRNAs generated by IR*Alu* pairing. This mechanism may be particularly relevant for tumors of tissues that accumulate large amounts of circRNAs, such as the cerebellum. Thus, although a role for hnRNP C as repressor of innate immunity was already proposed in other cancer types (*40*, *41*), here, we demonstrate that this dsRNA-induced antiviral response can be generated by pairing of intronic RNA sequences involved in back-splicing reactions. In support of this notion, our bioinformatics analyses did not show an enrichment in IR events into linear transcripts in hnRNP C–depleted cells that could justify the accumulation of cytoplasmic dsRNAs observed upon hnRNP C depletion (fig. S3G). Furthermore, in vitro functional studies using SMN2 minigenes showed that introns flanking hnRNP C–regulated BSJs mostly contribute to the accumulation of cytoplasmic dsRNAs. The increase of minigene-derived SMN2 circRNA was associated with increased cytoplasmic accumulation of J2-immunoprecipitated dsRNAs upon hnRNP C depletion. The PdB treatment increased the retention of minigene-derived intron 5, which is the upstream intron of BSJ, but its higher expression with respect to untreated cells was not sufficient to increase the cytoplasmic dsRNAs into the cells. Even if we cannot completely rule out that some of the cytoplasmic dsRNAs are generated from hnRNP C–dependent IR events, our data strongly suggest that these molecules can also be generated by introns that anneal in the course of circRNA biogenesis.

In conclusion, our study uncovers a key role of hnRNP C in maintenance of the transcriptome integrity by binding IR*Alu* elements in nascent RNAs and limiting their pairing and circRNA biogenesis. Thus, if on one hand hnRNP C prevents the exonization of *Alu* elements into the coding transcriptome (*33*), it also contributes to this process by repressing the circularization of the *Alu*-containing pre-mRNAs. In both cases, the lack of hnRNP C increases cytoplasmic accumulation of dsRNAs and activates a viral mimicry response. It remains to be investigated how these RNA adducts are transported from the nucleus into the cytoplasm, whether and how they are stabilized, and whether their specific structure (opened at both ends) requires a different repertoire of innate immunity sensors. Further studies will also be required to elucidate the functional role of hnRNP C–regulated circRNAs on the phenotype(s) of cerebellar cells and how their global reduction affects group 3 MB cells. Moreover, as RBPs are emerging as therapeutic targets for diseases involving genomic abnormalities such as cancer (*42*), inhibiting hnRNP C or enhancing the back-splicing–deriving dsRNAs could represent innovative methods to activate an immune response against MB.

MATERIALS AND METHODS

Human cell lines

D341-Med (D341) and HD-MB03 cells were cultured according to the recommended conditions (American Type Culture Collection). D341 cells were cultured in minimal essential medium (MEM; Gibco) supplemented with 1 mM sodium pyruvate (Gibco), 1X MEM non-essential amino acids solution (Gibco), 20% fetal bovine serum (FBS; Gibco), penicillin (100 U/ml), and streptomycin (10 μg/ml; Euroclone). HD-MB03 cells (obtained from Deutsche Sammlung von Mikroorganismen und Zellkulturen DSMZ, Germany) were maintained in RPMI (Gibco) with 10% FBS (Gibco), penicillin (100 U/ml), and streptomycin (100 μg/ml; Euroclone). HEK293T cells were maintained in Dulbecco MEM (Sigma-Aldrich) supplemented with 1X MEM non-essential amino acids solution (Gibco), 10% FBS (Gibco), penicillin (100 U/ml), and streptomycin (100 μg/ml; Euroclone). All cell lines were cultured at 37°C in a humidified atmosphere with 5% CO_2 and tested for mycoplasma contamination by PCR every 3 months. HEK293T was treated with 10 nM Pladienolide B (catalog no. 391691, Santa Cruz Biotechnology) for 6 hours.

Cell transfections

Cells were transfected with 50 nM specific siRNAs using Lipofectamine RNAiMax Transfection Reagent (catalog no. 13778150, Invitrogen) according to the manufacturer's instructions. The following siRNAs were used in this study: HNRNPC (siRNA#1, HSS179304; siRNA#2, HSS179305) (Stealth siRNAs, Thermo Fisher Scientific), SART3 (siRNA#1, SASI_Hs01_00115659; siRNA#2, SASI_Hs01_00115660) (siRNA pre-designed, Merck), KHDRBS1/Sam68 (ON-TARGETplus siRNA Smartpool L-020019-00, Horizon), KHDRBS2/SLM1 (target sequence GUGCAUGCGUCGCGCCUUU, purchased as custom siRNA from Merck), and DHX9 (target sequence, AAGAAGUGCAAGCGACUCUAG, purchased as custom siRNA from Merck). Nontargeting scrambled siRNAs were used as negative control. RNA and proteins were extracted 72 hours after transfection, unless stated otherwise in the text. HEK293T cells were transfected using Lipofectamine 2000 transfection reagent (catalog no. 11668019, Invitrogen) according to the manufacturer's instructions.

Western blot analysis and antibodies

Cells were lysed in radioimmunoprecipitation assay buffer [1% NP-40, 0.1% SDS, 150 mM NaCl, 50 mM tris-HCl (pH 7.5), and 0.5% sodium deoxycholate] supplemented with 1% protease inhibitor cocktail (Sigma-Aldrich), 0.5 mM Na_3VO_4, 1 mM dithiothreitol (DTT). Equal amounts of proteins were separated on SDS–polyacrylamide gel electrophoresis gels, transferred to polyvinylidene difluoride membranes (Bio-Rad), and probed with the following antibodies: anti-HNRNPC (catalog no. 91327S, Cell Signaling Technology), anti-SART3 (catalog no. GTX107684, GeneTex), anti-KHDRBS1/Sam68 (catalog no. A302-110A, Bethyl Laboratories), anti-HSP90 (catalog no. sc-13119, Santa Cruz Biotechnology), anti-histone H3 (catalog no. 17168-1-AP, Proteintech), and anti-DHX9 (catalog no. A300-855A, Bethyl Laboratories). Anti-KHDRBS2/SLM1 was gently provided by P. Scheiffele (University of Basel, Switzerland). Detection was achieved by using anti-mouse horseradish peroxidase (HRP) conjugated (catalog no. NA931, Amersham), and anti-rabbit HRP conjugated (catalog no. NA934, Amersham) and visualized by Clarity Western ECL Substrate (catalog no. 1705061, Bio-Rad).

Total RNA extraction and quantitative real-time PCR analyses

Total RNA was extracted using miRNeasy mini kit (catalog no. 217004, QIAGEN) according to the manufacturer's instructions. Total RNA was retrotranscribed with random primers using M-MLV reverse transcriptase (Promega) according to the manufacturer's instructions. For circRNA detection, total RNA was treated with 2 U of RNase R (catalog no. RNR07250, Biosearch Technologies) per μg of RNA for 20 min at 37°C. qPCR was carried out using LightCycler 480 SYBR Green I Master and the LightCycler 480 System (Roche),

according to the manufacturer's instructions. Divergent primer pairs encompassing the BSJ were used to detect circRNAs. The complete list of all primers used in this study is provided in table S22.

UV CLIP assay

CLIP assays were performed as described in (*43*). D341 cells were UV-irradiated on ice (100 mJ/cm^2). Following irradiation, cells were pelleted by centrifugation at 4000 rpm for 5 min. The resulting pellet was lysed on ice for 10 min in lysis buffer containing 50 mM tris (pH 8.0), 100 mM NaCl, 1% NP-40, 1 mM $MgCl_2$, 0.1 mM $CaCl_2$, 0.5 mM Na_3VO_4, 1 mM DTT, a protease inhibitor cocktail (Sigma-Aldrich), and RNase inhibitor (Promega). Lysates were briefly sonicated and subsequently treated with RNase-free deoxyribonuclease (DNase) (Ambion) for 3 min at 37°C. After DNase treatment, samples were centrifuged at 15.000*g* for 3 min at 4°C. For input RNA extraction, 0.1 mg of total extract was incubated with proteinase K at 55°C for 30 min, and RNA was purified using standard protocols. For immunoprecipitation, 1 mg of extract was diluted to 1 ml in lysis buffer and incubated with 3 μg of anti–hnRNP C antibody (catalog no. 91327S, Cell Signaling Technology) or control immunoglobulin Gs (IgGs), along with protein G magnetic Dynabeads (Life Technologies). RNase I (1000 IU; Ambion) was added, and samples were incubated for 2 hours at 4°C with continuous rotation. After stringent washes (*43*), 10% of the immunoprecipitate was retained as an IP control. The remaining fraction was digested with 50 μg of proteinase K at 55°C for 1 hour, and RNA was isolated following standard procedures.

Plasmid constructs

circSMN minigene was generated as previously described (*7*). For mutagenesis of hnRNP C binding site (BS) 1, a megaprimer containing 13 T>A at BS1 was amplified using primers #1 and #2 and circSMN minigene as a template. Megaprimer and primers #3 were used to amplify 5′ end of circSMN minigenes containing the mutagenized BS1. For mutagenesis of hnRNP C BS2, a second megaprimer with 12 T>A at BS2 was obtained with primers #3 and #4 and then used with primer #1 to amplify the 5′ end of circSMN with mutated BS2. Double mutant (BS1 and BS2) was generated by using the same megaprimer-based strategy and circSMN BS2 mutant as template. All PCR amplicons generated for the mutations were digested with Kpn I and Sal I restriction enzymes for cloning into initial circSMN plasmid digested with the same enzymes. PCR primers listed in table S22.

Cellular fractionation experiments

Following siRNA transfection for 72 hours, HD-MB03 cell pellet collected from two 10-cm dishes was lysed in a buffer containing 10 mM tris-HCl (pH 7.5), 0.15% NP-40, and 150 mM NaCl supplemented with 2 mM sodium orthovanadate, 1 mM DTT, and 1% protease inhibitor cocktail (Sigma-Aldrich), allowing plasma membrane disruption. After 15-min incubation on ice, the lysate was layered over a chilled sucrose cushion [24% (w/v) in lysis buffer, 2.5 vol] and centrifuged at 14.000 rpm for 10 min at 4°C. The supernatant containing the cytoplasmic fraction was collected. A 50 μl of cytoplasmic fraction was treated with 5 U of RNase III (catalog no. AM2290, Invitrogen) at 37°C for 30 min, while the same volume (50 μl) was left untreated at 37°C for 30 min. Cytoplasmic fractions were then resuspended in 20 volumes of QIAzol (QIAGEN) and RNA extracted using the miRNeasy mini kit (catalog no. 217004, QIAGEN) according to the manufacturer's instructions. The nuclear pellet was gently rinsed with cold phosphate-buffered saline (PBS), treated with RNase III for 30 min at 37°C, and then resuspended in QIAzol for nuclear RNA extraction.

Immunoprecipitation assay with anti-dsRNA J2 antibody

Cytoplasmic RNA from HD-MB03 cells silenced or not for the expression of hnRNP C was obtained as above. Contaminating DNA was removed by DNase treatment (TURBO DNA-free, Thermo Fisher Scientific). Phenol-chloroform–purified RNA was then subjected to immunoprecipitation using the anti-dsRNA J2 antibody (catalog no. 76651, Cell Signaling Technology). Briefly, 100 μg of cytosolic RNA was diluted in 1 ml of freshly prepared IP lysis buffer [5 mM tris-HCl (pH 7.4), 150 mM NaCl, 1 mM EDTA, 1% NP-40, and 5% glycerol] supplemented with RNase inhibitor (20 U/ml) and 1 mM phenylmethylsulfonyl fluoride. To reduce nonspecific binding, RNA samples were precleared by incubation with 50 μl of Dynabeads Protein G (catalog no. 10004D, Thermo Fisher Scientific) for 30 min at 4°C with continuous rotation. After the removal of the Dynabeads, 10 μg of RNA was collected from the supernatant and used as input (10%). The remaining supernatant was equally divided into two fractions and incubated overnight at 4°C with either 10 μg of anti-dsRNA J2 antibody or an equal amount of IgG control, with continuous rotation. After, 40 μl of Dynabeads Protein G was added to each reaction and incubated for an additional 2 hours at 4°C with continuous rotation. Beads were then collected and washed five times with 800 μl of prechilled 1× tris-buffered saline [50 mM tris-HCl (pH 7.4) and 150 mM NaCl]. Last, RNA co-immunoprecipitated with the beads was purified using TRIzol reagent and resuspended in 14 μl of nuclease-free water for reverse transcription.

Immunofluorescence assay

HD-MB03 cells were washed in PBS, fixed with 4% (v/v) formaldehyde for 15 min at room temperature, washed three times with PBS, permeabilized with 0.5% (v/v) Triton X-100 in PBS for 15 min at room temperature, and washed twice with PBS. Cells were incubated with blocking solution (3% bovine serum albumin in PBS) for 45 min at room temperature before incubation with anti-dsRNA J2 antibody (catalog no. 76651, Cell Signaling Technology) at 4°C overnight. Cells were washed three times with PBS before incubation with secondary antibody (Alexa Fluor 488, catalog no. A11029, Thermo Fisher Scientific) for 1 hour at room temperature. Cells were again washed three times with PBS, and the nuclei were stained using 4′,6′-diamidino-2-phenylindole. Coverslips were mounted with VECTASHIELD mounting medium. Images were analyzed by ImageJ software.

Cell viability assay

Cell viability was assessed by CellTiter 96 AQueous One Solution Cell Proliferation Assay ([3-(4,5-dimethylthiazol-2-yl)-5-(3-carboxymethoxyphenyl)-2-(4-sulfophenyl)-2H-tetrazolium, inner salt; catalog no. G3582, Promega] and performed in 96-well plates. For D341 cell line, 10,000 cells per well were seeded. For HD-MB03 cell line, 3000 cell per well were seeded. The assay was performed by adding 20 μl of the CellTiter 96 AQueous One Solution Reagent directly to culture wells, incubating for 2 to 4 hours and then recording absorbance at 490 nm with a 96-well plate reader (iMark Microplate Absorbance Reader, Bio-Rad). The quantity of formazan product as measured by the amount of 490-nm absorbance was directly proportional to the number of living cells in culture.

Spheroid assay

D341 cells were transfected with siHNRNPC#1, siHNRNPC#2, or control siRNA for 24 hours. Cells were then trypsinised, resuspended in MEM full media containing 0.24% methyl cellulose (catalog no. M7027, Merck), and seeded in round bottom ultra-low attachment 96 well plate (catalog no. 7007, Corning) (250 cells per well). Plates were centrifuged at 100*g* for 5 min to allow cells to settle at the bottom of the wells. The growth of spheroids were monitored at different time points using microplate multichannel automated imaging Celigo Image Cytometer (Nexcelom Bioscience) to assess changes in area and fluorescence intensity. Note that the average mean fluorescent intensity (MFI) represents the averages of the MFI of the four replicate spheroids.

RNA-seq samples alignment and back-splicing events calling in patients with group 3 MB

Calling of BS events was done using two distinct methods: CIRCexplorer2 version 2.3.8 (*24*) and CIRI version 2.1.1 (*25*). For the CIRCexplorer2 pipeline, EGA FASTQ samples (EGAD00001004958 dataset; DACO-1766 approved application ID at International Cancer Genome Consortium platform) from MB, FC, and AC were downloaded from https://ega-archive.org and initially aligned to detect chimeric junctions using the STAR algorithm version 2.7.9a (*44*), with the following settings:

```
STAR \
--readFilesIn fastq1 fastq2 \
--runThreadN 16 \
--genomeDir STAR_HG19 \
--readFilesCommand zcat \
--outSAMtype BAM SortedByCoordinate \
--quantMode GeneCounts \
--chimSegmentMin 10 \
--outFileNamePrefix EGAF0000xxxxxxx_xx
```

where "fastq1" and "fastq2" refer to the fastq.gz read pair files, "STAR_HG19" is a directory containing the FASTA chromosome files for the human genome assembly GRCh37 (hg19), and a custom prefix is used, in the form EGAF0000xxxxxxx_xx, reflecting the EGA sample identifier. BS events were directly called and annotated from STAR chimeric junctions using CIRCExplorer2:

```
CIRCexplorer2 parse -t STAR EGAF0000xxxxxxxChimeric.out.junction > EGAF0000xxxxxxxCE2_parse.log
CIRCexplorer2 annotate \
-r hg19_ref_all.txt \
-g GENCODEv19/GRCh37.p13.genome.fa \
-b back_spliced_junction.bed \
-o EGAF0000xxxxxxx_circularRNA.txt
```

The "hg19_ref_all.txt" file is a collection of transcripts loci from UCSC Known Genes, RefSeq, and Ensembl transcripts, retrieved from the UCSC Genome Browser (*45*) database (last access: June 2022). GENCODE data and GRCh37 assembly FASTA files were also retrieved from the UCSC Genome Browser database.

For the CIRI pipeline, GRCh37 genome FASTA was indexed, and raw reads were aligned using the Burrows-Wheeler Aligner-Maximal Exact Matches (BWA-MEM) algorithm (*46*). The whole CIRI pipeline, including annotation, was run using the following settings:

```
java -jar /apps/ciri/2.1.1/bin/CIRI_Full_v2.1.1.jar \
-1 fastq1.fastq.gz \
-2 fastq2.fastq.gz \
-r GENCODEv19/GRCh37.p13.genome.fa \
-a GENCODEv19/gencode.v19.annotation.gtf \
-t 16 \
-d EGAF0000xxxxxxx_xx \
-o EGAF0000xxxxxxx_xx
```

The overlap between CIRCexplorer2 and CIRI calls is our high confidence BS set.

BSJ quantification and differential junction usage

For CIRIquant analysis, BWA, HISAT2, StringTie, and Samtools were used, and CIRIquant was used for quantification of circRNAs with the default parameters.

For circRNA differential expression analysis between MB and FC or AC samples, we used prep_CIRIquant to summarize the circRNA expression profile in all samples obtained from CIRIquant and then prepDE.py and CIRI_DE_replicate for circRNA differential expression analyses using default parameters.

Linear splicing and back-splicing analyses in hnRNP C–depleted MB cells

For linear splicing analyses, please refer to (*47*, *48*). BSJs were identified using CIRI-full algorithm (*49*), and CIRIquant (*50*) was used for quantification and differential analysis, with RNAse-treated and -untreated samples. Annotations of circRNAs were done using GRCh38 genome and GENCODE v32 annotations. circRNAs were detected in RNase-treated samples, but quantification was done on untreated samples to evaluate and take into account the efficiency of RNAse treatment (CIRIquant option). A circRNA was considered expressed in one sample if it has at least two reads on BSJ. A circRNA was expressed in one condition if it is expressed in at least half of the samples of the condition. A unique circRNA is a circRNA expressed in one sample only. For circular to linear ratio, the value was calculated by CIRI, and only circRNA detected in all samples were reported.

Introns flanking BSJs from up-regulated and unregulated circRNAs were identified using FAST DB v2022_1 annotations. *Alu* definition was downloaded from UCSC using the "rmsk" table from the hg38 database. Inter-intronic IR*Alu*s were defined as pair of *Alu* sequences with each *Alu* from a given pair on one of the two BSJ flanking introns and on the opposite direction. Each *Alu* sequence was counted once (i.e., a given *Alu* was not shared in several inter-intronic IR*Alu*s).

The number of inter-intronic IR*Alu*s per intron between BSJ flanking introns was compared with those within pairs of introns with similar length from expressed genes and from genes with BSJ but not BSJ flanking introns (to avoid bias due to intron length variation). Strong hnRNP C–binding motif was defined as polyT with at least nine "T." Intron sequences were screened for hnRNP C motifs using a Perl script. Distances between hnRNP C motifs and BSJ or *Alu* were determined using R and Perl scripts.

Analysis of RNA binding motifs

Sequence analysis for enriched motifs in intronic regions flanking splice sites involved circRNA biogenesis in AC was performed using the sequence motif discovery algorithm STREME (https://meme-suite.org/meme/) (*26*). A 4- to 7-nt-long motifs statistically significantly enriched ($P \leq 0.05$) were searched by comparative analyses of 100-nt-long sequences upstream of the 5′ and 3′ splice sites of BSJs with those of analogous sequences from introns involved in canonical splicing events. The comparison of enriched motifs with the database

from (*29*) of known binding sites for RBPs was performed using the Tomtom tool (*28*).

HnRNP C iCLIP-seq data analyses

hnRNP C iCLIP-seq data, from previously published dataset (*36*), were downloaded from the EMBL-EBI ArrayExpress (www.ebi.ac.uk/arrayexpress/) under the accession code E-MTAB-1371 and analyzed as described (*36*). The proportion of hnRNP C binding on *Alu* elements genome-wide was performed with the findOverlaps function of GenomicRanges R package (v1.44.0) by using the iCLIP peak coordinates and the *Alu* repeat family coordinates, downloaded from UCSC, and the "rmsk" table from the hg38 database. Proportion of the introns flanking the detected BSJs and the up-regulated BSJs was performed with the findOverlaps function of GenomicRanges R package using the iCLIP peak coordinates overlapping *Alu* elements and the BSJ intron coordinates.

Statistical analyses

GraphPad Prism software was used for statistical analysis. Data are presented as means ± SD unless stated otherwise. Comparisons between groups were made using Student's *t* test, Welch's *t* test, or analysis of variance (ANOVA) as appropriate and as indicated in figure legends.

Supplementary Materials

This PDF file includes:

Figs. S1 to S5

Legends for tables S1 to S22

REFERENCES

1. X. Li, L. Yang, L. L. Chen, The biogenesis, functions, and challenges of circular RNAs. *Mol. Cell* **71**, 428–442 (2018).
2. C. R. Sibley, L. Blazquez, J. Ule, Lessons from non-canonical splicing. *Nat. Rev. Genet.* **17**, 407–421 (2016).
3. C. Pitolli, A. Marini, C. Sette, V. Pagliarini, Non-canonical splicing and its implications in brain physiology and cancer. *Int. J. Mol. Sci.* **23**, 2811 (2022).
4. V. M. Conn, A. M. Chinnaiyan, S. J. Conn, Circular RNA in cancer. *Nat. Rev. Cancer* **24**, 597–613 (2024).
5. X. O. Zhang, H.-B. Wang, Y. Zhang, X. Lu, L. L. Chen, L. Yang, Complementary sequence-mediated exon circularization. *Cell* **159**, 134–147 (2014).
6. S. J. Conn, K. A. Pillman, J. Toubia, V. M. Conn, M. Salmanidis, C. A. Phillips, S. Roslan, A. W. Schreiber, P. A. Gregory, G. J. Goodall, The RNA binding protein quaking regulates formation of circRNAs. *Cell* **160**, 1125–1134 (2015).
7. V. Pagliarini, A. Jolly, P. Bielli, V. Di Rosa, P. De La Grange, C. Sette, Sam68 binds *Alu*-rich introns in SMN and promotes pre-mRNA circularization. *Nucleic Acids Res.* **48**, 633–645 (2020).
8. D. Knupp, D. A. Cooper, Y. Saito, R. B. Darnell, P. Miura, NOVA2 regulates neural circRNA biogenesis. *Nucleic Acids Res.* **49**, 6849–6862 (2021).
9. L. V. W. Stagsted, E. T. O'leary, K. K. Ebbesen, T. B. Hansen, The RNA-binding protein SFPQ preserves long-intron splicing and regulates circrna biogenesis in mammals. *eLife* **10**, e63088 (2021).
10. R. K. Bradley, O. Anczuków, RNA splicing dysregulation and the hallmarks of cancer. *Nat. Rev. Cancer* **23**, 135–155 (2023).
11. J. N. Vo, M. Cieslik, Y. Zhang, S. Shukla, L. Xiao, Y. Zhang, Y. M. Wu, S. M. Dhanasekaran, C. G. Engelke, X. Cao, D. R. Robinson, A. I. Nesvizhskii, A. M. Chinnaiyan, The landscape of circular RNA in cancer. *Cell* **176**, 869–881.e13 (2019).
12. D. Rickert, J. Bartl, D. Picard, F. Bernardi, N. Qin, M. Lovino, S. Puget, F. D. Meyer, I. Mahoungou Koumba, T. Beez, P. Varlet, C. Dufour, U. Fischer, A. Borkhardt, G. Reifenberger, O. Ayrault, M. Remke, Circular RNA profiling distinguishes medulloblastoma groups and shows aberrant RMST overexpression in WNT medulloblastoma. *Acta Neuropathol.* **141**, 975–978 (2021).
13. F. M. G. Cavalli, M. Remke, L. Rampasek, J. Peacock, D. J. H. Shih, B. Luu, L. Garzia, J. Torchia, C. Nor, A. S. Morrissy, S. Agnihotri, Y. Y. Thompson, C. M. Kuzan-Fischer, H. Farooq, K. Isaev, C. Daniels, B. K. Cho, S. K. Kim, K. C. Wang, J. Y. Lee, W. A. Grajkowska, M. Perek-Polnik, A. Vasiljevic, C. Faure-Conter, A. Jouvet, C. Giannini, A. A. Nageswara Rao, K. K. W. Li, H. K. Ng, C. G. Eberhart, I. F. Pollack, R. L. Hamilton, G. Y. Gillespie, J. M. Olson, S. Leary, W. A. Weiss, B. Lach, L. B. Chambless, R. C. Thompson, M. K. Cooper, R. Vibhakar, P. Hauser, M. L. C. van Veelen, J. M. Kros, P. J. French, Y. S. Ra, T. Kumabe, E. López-Aguilar, K. Zitterbart, J. Sterba, G. Finocchiaro, M. Massimino, E. G. van Meir, S. Osuka, T. Shofuda, A. Klekner, M. Zollo, J. R. Leonard, J. B. Rubin, N. Jabado, S. Albrecht, J. Mora, T. E. van Meter, S. Jung, A. S. Moore, A. R. Hallahan, J. A. Chan, D. P. C. Tirapelli, C. G. Carlotti, M. Fouladi, J. Pimentel, C. C. Faria, A. G. Saad, L. Massimi, L. M. Liau, H. Wheeler, H. Nakamura, S. K. Elbabaa, M. Perezpeña-Diazconti, F. Chico Ponce de León, S. Robinson, M. Zapotocky, A. Lassaletta, A. Huang, C. E. Hawkins, U. Tabori, E. Bouffet, U. Bartels, P. B. Dirks, J. T. Rutka, G. D. Bader, J. Reimand, A. Goldenberg, V. Ramaswamy, M. D. Taylor, Intertumoral heterogeneity within medulloblastoma subgroups. *Cancer Cell* **31**, 737–754.e6 (2017).
14. P. A. Northcott, G. W. Robinson, C. P. Kratz, D. J. Mabbott, S. L. Pomeroy, S. C. Clifford, S. Rutkowski, D. W. Ellison, D. Malkin, M. D. Taylor, A. Gajjar, S. M. Pfister, Medulloblastoma. *Nat. Rev. Dis. Primer* **5**, 11 (2019).
15. A. Rybak-Wolf, C. Stottmeister, P. Glažar, M. Jens, N. Pino, S. Giusti, M. Behm, O. Bartok, R. Ashwal-Fluss, M. Herzog, L. Schreyer, P. Papavasileiou, A. Ivanov, M. Öhman, D. Refojo, S. Kadener, N. Rajewsky, Circular RNAs in the mammalian brain are highly abundant, conserved, and dynamically expressed. *Mol. Cell* **58**, 870–885 (2015).
16. T. Y. T. Hsu, L. M. Simon, N. J. Neill, R. Marcotte, A. Sayad, C. S. Bland, G. V. Echeverria, T. Sun, S. J. Kurley, S. Tyagi, K. L. Karlin, R. Dominguez-Vidaña, J. D. Hartman, A. Renwick, K. Scorsone, R. J. Bernardi, S. O. Skinner, A. Jain, M. Orellana, C. Lagisetti, I. Golding, S. Y. Jung, J. R. Neilson, X. H. F. Zhang, T. A. Cooper, T. R. Webb, B. G. Neel, C. A. Shaw, T. F. Westbrook, The spliceosome is a therapeutic vulnerability in MYC-driven cancer. *Nature* **525**, 384–388 (2015).
17. L. Urbanski, M. Brugiolo, S. H. Park, B. L. Angarola, N. K. Leclair, M. Yurieva, P. Palmer, S. K. Sahu, O. Anczuków, MYC regulates a pan-cancer network of co-expressed oncogenic splicing factors. *Cell Rep.* **41**, 111704 (2022).
18. C. J. David, M. Chen, M. Assanah, P. Canoll, J. L. Manley, HnRNP proteins controlled by c-Myc deregulate pyruvate kinase mRNA splicing in cancer. *Nature* **463**, 364–368 (2010).
19. S. Das, O. Anczuków, M. Akerman, A. R. Krainer, Oncogenic splicing factor SRSF1 is a critical transcriptional target of MYC. *Cell Rep.* **1**, 110–117 (2012).
20. C. Caggiano, M. Pieraccioli, V. Panzeri, C. Sette, P. Bielli, C-MYC empowers transcription and productive splicing of the oncogenic splicing factor Sam68 in cancer. *Nucleic Acids Res.* **47**, 6160–6171 (2019).
21. R. Ashwal-Fluss, M. Meyer, N. R. Pamudurti, A. Ivanov, O. Bartok, M. Hanan, N. Evantal, S. Memczak, N. Rajewsky, S. Kadener, CircRNA biogenesis competes with Pre-mRNA splicing. *Mol. Cell* **56**, 55–66 (2014).
22. Y. Zhang, W. Xue, X. Li, J. Zhang, S. Chen, J. L. Zhang, L. Yang, L. L. Chen, The biogenesis of nascent circular RNAs. *Cell Rep.* **15**, 611–624 (2016).
23. D. Liang, D. C. Tatomer, Z. Luo, H. Wu, L. Yang, L. L. Chen, S. Cherry, J. E. Wilusz, The output of protein-coding genes shifts to circular RNAs when the pre-mRNA processing machinery is limiting. *Mol. Cell* **68**, 940–954.e3 (2017).
24. X. O. Zhang, R. Dong, Y. Zhang, J. L. Zhang, Z. Luo, J. Zhang, L. L. Chen, L. Yang, Diverse alternative back-splicing and alternative splicing landscape of circular RNAs. *Genome Res.* **26**, 1277–1287 (2016).
25. Y. Gao, J. Wang, F. Zhao, CIRI: An efficient and unbiased algorithm for de novo circular RNA identification. *Genome Biol.* **16**, 1–16 (2015).
26. T. L. Bailey, M. Boden, F. A. Buske, M. Frith, C. E. Grant, L. Clementi, J. Ren, W. W. Li, W. S. Noble, MEME Suite: Tools for motif discovery and searching. *Nucleic Acids Res.* **37**, W202–W208 (2009).
27. T. L. Bailey, STREME: Accurate and versatile sequence motif discovery. *Bioinformatics* **37**, 2834–2840 (2021).
28. S. Gupta, J. A. Stamatoyannopoulos, T. L. Bailey, W. S. Noble, Quantifying similarity between motifs. *Genome Biol.* **8**, R24 (2007).
29. D. Ray, H. Kazan, K. B. Cook, M. T. Weirauch, H. S. Najafabadi, X. Li, S. Gueroussov, M. Albu, H. Zheng, A. Yang, H. Na, M. Irimia, L. H. Matzat, R. K. Dale, S. A. Smith, C. A. Yarosh, S. M. Kelly, B. Nabet, D. Mecenas, W. Li, R. S. Laishram, M. Qiao, H. D. Lipshitz, F. Piano, A. H. Corbett, R. P. Carstens, B. J. Frey, R. A. Anderson, K. W. Lynch, L. O. F. Penalva, E. P. Lei, A. G. Fraser, B. J. Blencowe, Q. D. Morris, T. R. Hughes, A compendium of RNA-binding motifs for decoding gene regulation. *Nature* **499**, 172–177 (2013).
30. A. Di Liddo, C. De Oliveira Freitas Machado, S. Fischer, S. Ebersberger, A. W. Heumüller, J. E. Weigand, M. Müller-Mcnicoll, K. Zarnack, A combined computational pipeline to detect circular RNAs in human cancer cells under hypoxic stress. *J. Mol. Cell Biol.* **11**, 829–844 (2019).
31. A. F. Nielsen, A. Bindereif, I. Bozzoni, M. Hanan, T. B. Hansen, M. Irimia, S. Kadener, L. S. Kristensen, I. Legnini, M. Morlando, M. T. Jarlstad Olesen, R. J. Pasterkamp, S. Preibisch, N. Rajewsky, C. Suenkel, J. Kjems, Best practice standards for circular RNA research. *Nat. Methods* **19**, 1208–1220 (2022).
32. Z. Cieniková, S. Jayne, F. F. Damberger, F. H. T. Allain, C. Maris, Evidence for cooperative tandem binding of hnRNP C RRMs in mRNA processing. *RNA* **21**, 1931–1942 (2015).

33. K. Zarnack, J. König, M. Tajnik, I. Martincorena, S. Eustermann, I. Stévant, A. Reyes, S. Anders, N. M. Luscombe, J. Ule, Direct competition between hnRNP C and U2AF65 protects the transcriptome from the exonization of Alu elements. *Cell* **152**, 453–466 (2013).
34. T. Aktaş, I. A. Ilik, D. Maticzka, V. Bhardwaj, C. Pessoa Rodrigues, G. Mittler, T. Manke, R. Backofen, A. Akhtar, DHX9 suppresses RNA processing defects originating from the Alu invasion of the human genome. *Nature* **544**, 115–119 (2017).
35. D. L. Court, J. Gan, Y. H. Liang, G. X. Shaw, J. E. Tropea, N. Costantino, D. S. Waugh, X. Ji, RNase III: Genetics and function: Structure and mechanism. *Annu. Rev. Genet.* **47**, 405–431 (2013).
36. C. Naro, A. Antonioni, V. Medici, C. Caggiano, A. Jolly, P. de la Grange, P. Bielli, M. P. Paronetto, C. Sette, Splicing targeting drugs highlight intron retention as an actionable vulnerability in advanced prostate cancer. *J. Exp. Clin. Cancer Res.* **43**, 58 (2024).
37. C. Caggiano, V. Petrera, M. Ferri, M. Pieraccioli, E. Cesari, A. Di Leone, M. A. Sanchez, A. Fabi, R. Masetti, C. Naro, C. Sette, Transient splicing inhibition causes persistent DNA damage and chemotherapy vulnerability in triple-negative breast cancer. *Cell Rep.* **43**, 114751 (2024).
38. O. Saulnier, J. Zagozewski, L. Liang, L. D. Hendrikse, P. Layug, V. Gordon, K. A. Aldinger, P. Haldipur, S. Borlase, L. Coudière-Morrison, T. Cai, E. Martell, N. M. Gonzales, G. Palidwor, C. J. Porter, S. Richard, T. Sharif, K. J. Millen, B. W. Doble, M. D. Taylor, T. E. Werbowetski-Ogilvie, A group 3 medulloblastoma stem cell program is maintained by OTX2-mediated alternative splicing. *Nat. Cell Biol.* **26**, 1233–1246 (2024).
39. C. Pitolli, A. Marini, M. Guerra, M. Pieraccioli, V. Marabitti, F. Palluzzi, L. Giacò, G. Tamburrini, F. Cecconi, F. Nazio, C. Sette, V. Pagliarini, MYC up-regulation confers vulnerability to dual inhibition of CDK12 and CDK13 in high-risk Group 3 medulloblastoma. *J. Exp. Clin. Cancer Res.* **42**, 214 (2023).
40. Y. Wu, W. Zhao, Y. Liu, X. Tan, X. Li, Q. Zou, Z. Xiao, H. Xu, Y. Wang, X. Yang, Function of HNRNPC in breast cancer cells by controlling the dsRNA-induced interferon response. *EMBO J.* **37**, 1–19 (2018).
41. A. M. Herzner, Z. Khan, E. L. van Nostrand, S. Chan, T. Cuellar, R. Chen, X. Pechuan-Jorge, L. Komuves, M. Solon, Z. Modrusan, B. Haley, G. W. Yeo, T. W. Behrens, M. L. Albert, ADAR and hnRNPC deficiency synergize in activating endogenous dsRNA-induced type I IFN responses. *J. Exp. Med.* **218**, e20201833 (2021).
42. S. Mohibi, X. Chen, J. Zhang, Cancer the'RBP'eutics–RNA-binding proteins as therapeutic targets for cancer. *Pharmacol. Ther.* **203**, 107390 (2019).
43. P. Bielli, C. Sette, Analysis of in vivo Interaction between RNA binding proteins and their RNA targets by UV cross-linking and immunoprecipitation (CLIP) method. *Bio Protocol* **7**, e2274 (2017).
44. A. Dobin, C. A. Davis, F. Schlesinger, J. Drenkow, C. Zaleski, S. Jha, P. Batut, M. Chaisson, T. R. Gingeras, STAR: Ultrafast universal RNA-seq aligner. *Bioinformatics* **29**, 15–21 (2013).
45. W. James Kent, C. W. Sugnet, T. S. Furey, K. M. Roskin, T. H. Pringle, A. M. Zahler, D. Haussler, The human genome browser at UCSC. *Genome Res.* **12**, 996–1006 (2002).
46. H. Li, R. Durbin, Fast and accurate short read alignment with Burrows-Wheeler transform. *Bioinformatics* **25**, 1754–1760 (2009).
47. E. Cesari, A. Ciucci, M. Pieraccioli, C. Caggiano, C. Nero, D. Bonvissuto, F. Sillano, M. Buttarelli, A. Piermattei, M. Loverro, F. Camarda, V. Greco, M. de Bonis, A. Minucci, D. Gallo, A. Urbani, G. Vizzielli, G. Scambia, C. Sette, Dual inhibition of CDK12 and CDK13 uncovers actionable vulnerabilities in patient-derived ovarian cancer organoids. *J. Exp. Clin. Cancer Res.* **42**, 126 (2023).
48. V. Ruta, C. Naro, M. Pieraccioli, A. Leccese, L. Archibugi, E. Cesari, V. Panzeri, C. Allgöwer, P. G. Arcidiacono, M. Falconi, C. Carbone, G. Tortora, F. Borrelli, F. Attili, C. Spada, G. Quero, S. Alfieri, C. Doglioni, A. Kleger, G. Capurso, C. Sette, An alternative splicing signature defines the basal-like phenotype and predicts worse clinical outcome in pancreatic cancer. *Cell Rep. Med.* **5**, 101411 (2024).
49. Y. Zheng, P. Ji, S. Chen, L. Hou, F. Zhao, Reconstruction of full-length circular RNAs enables isoform-level quantification. *Genome Med.* **11**, 2 (2019).
50. J. Zhang, S. Chen, J. Yang, F. Zhao, Accurate quantification of circular RNAs identifies extensive circular isoform switching events. *Nat. Commun.* **11**, 90 (2020).

Acknowledgments: We wish to thank M. Guerra and V. Petrera for technical assistance and C. Caggiano for critical reading of the manuscript and helpful suggestions. We also thank all members of the laboratory for fruitful discussion throughout the course of this study. **Funding:** This work was funded by the following grants: Associazione Italiana Ricerca sul Cancro, AIRC (grant no. MFAG24767); the Progetti di Rilevante Interesse Nazionale, PRIN (grant no. P2022JLHZZ); the Fondazione MiaNeri to V.P; the Fondazione Umberto Veronesi to A.M.; the Associazione Italiana Ricerca sul Cancro, AIRC (project code 28286) to C.P.; and the Associazione Italiana Ricerca sul Cancro, AIRC (grant no. MFAG27019) to F.N. Università Cattolica del Sacro Cuore contributed to the funding of this research project and its publication. **Author contributions:** Conceptualization: V.P., C.S., A.M., and C.P. Methodology: A.M., C.P., S.C., C.N., M.G., and P.B. Software: M.P., N.R., C.N., F.P., L.G., and P.D.L.G. Validation: V.P., A.M., C.P., and S.C. Formal analysis: V.P., A.M., C.P., S.C., M.P., and P.d.l.G. Investigation: V.P., A.M., C.P., S.C., M.G., and P.B. Resources: V.P., C.S., G.T., F.N., and P.B. Data curation: A.M., M.P., N.R., C.N., F.P., L.G., and P.D.L.G. Writing—original draft: V.P., C.S., and A.M. Writing—review and editing: V.P. and C.S. Visualization: V.P., C.S., A.M., C.P., and S.C. Supervision: V.P. and C.S. Project administration: V.P. Funding acquisition: V.P. and C.S. **Competing interests:** The authors declare that they have no competing interests. **Data, code, and materials availability:** All data and code needed to evaluate and reproduce the conclusions in the paper are present in the paper and/or the Supplementary Materials. There are no new materials generated in the study. RNA-seq data are available on GEO database (accession number GSE304204). Tables S1 to S22 are available on Zenodo (https://doi.org/10.5281/zenodo.18385802).

Submitted 8 August 2025
Accepted 25 March 2026
Published 1 May 2026
10.1126/sciadv.aea2351